

# Upwind Reproducing Kernel Collocation Method for Convection-Dominated Problems

Jiarui Wang <sup>\*a,c</sup> and Michael Hillman<sup>b,c</sup>

<sup>a</sup>*School of Engineering, Brown University, 184 Hope St., Providence, RI 02912, USA*

<sup>b</sup>*Karagozian & Case, 700 N Brand Blvd, # 700, Glendale, CA 91203, USA.*

<sup>c</sup>*Department of Civil and Environmental Engineering, The Pennsylvania State University, University Park, PA 16802, USA.*

## Highlights

- Severe oscillations in node-based collocation methods have been found in convection-dominated problems
- Relationship between upwind stabilization and gradient smoothing technique is built
- Upwind reproducing kernel collocation method is designed
- No artificial parameter for stabilization is required in the entire formulation

## Abstract

Because of the best approximation property, traditional Bubnov-Galerkin numerical methods have proven immensely successful in modeling self-adjoint problems, such as heat conduction, elasticity, and so on. However, a numerical instability arises in these (and central finite difference) methods for problems with strong convection. In this class of problems, the convective transport term can lead to large spurious oscillations but can be handled by the class of Petrov-Galerkin methods. In particular, the upwind-type schemes and their variational and subgrid descendants have been substantially developed over the years for an effective weak-form Galerkin solution that precludes these instabilities. Nevertheless, the scale of development of upwind methods for strong-form collocation is substantially smaller, where numerical oscillations are also observed when they are straightforwardly applied to convection-dominated problems without special treatment. To this end, this paper presents a new upwind collocation method. First, the connection between the upwind finite difference scheme and the gradient smoothing technique in meshfree methods is established. It is then shown that selecting the collocation points as meshfree nodal points is not optimal; selecting the collocation points according to the flow direction and Péclet number is then studied. The upwind effect is achieved without introducing artificial parameters and is trivial to generalize for multi-dimensional cases. Cross-wind diffusion is also not observed in the solution. An error analysis is presented, and the effectiveness of the proposed methodology is well demonstrated by the steady and unsteady numerical examples.

**keywords** collocation, upwind, RKPM, convection-dominated problems

## 1 Introduction

The *best approximation* property possessed by the Bubnov-Galerkin method has been the key ingredient for the success of FEM in modeling the problems such as heat conduction and elasticity [1]. However, the convective transport terms in Eulerian conservation laws make the Bubnov-Galerkin method non-symmetric, leading to a loss of the "best approximation" property. Consequently, numerical solutions for problems with significant first-order convective terms may display spurious oscillations. One potential remedy for such oscillations is to refine the discretization or decrease the element Péclet number. Stabilized Petrov-Galerkin methods [2–4] have successfully mitigated the unstable oscillations in traditional Bubnov-Galerkin approaches by introducing artificial diffusivity. Additionally, alternative methods featuring fine-scale features, such as the variational multi-scale method and residual free bubbles [5] and residual free bubbles [6], have been developed to address challenges associated with Bubnov-Galerkin methods.

---

\*Corresponding author: jiarui\_wang@brown.edu

The numerical difficulties from the convection-dominated problems are also grounded in the class of meshfree methods. Developed over two decades ago [7], these methods have demonstrated success in modeling large deformations, penetration, and fragmentation [8, 9], achieving stability through nodal integration [10, 11]. Substantial efforts have been devoted to the development of stabilized meshfree methods for convection-dominated problems. The finite point method [12] was employed to solve convective transport and compressible flow problems under residual type stabilization. The multi-resolution reproducing kernel particle method (RKPM) [13] was emerged by combining the original RKPM [14] with the well-known streamline upwind Petrov-Galerkin (SUPG) method [3]. Another approach is the meshless local Petrov-Galerkin (MLPG) [15], designed to stabilize convection-dominated problems. This is achieved through either employing upwind-type test functions, akin to the concept proposed by Christie et al. [2], or modifying the support of the test function. The discussion of stabilization parameter between the meshfree and meshfree based methods was discussed in [16]. The upwind meshfree point interpolation collocation approach was proposed by Gu et al. [17], where the upwind stabilization was achieved by biasing the nodal support domain to the upwind region. Similar ideas have been employed in the development of meshfree upwind collocation method by using the radial basis function [18, 19]. The meshfree radial basis function has also been implemented to incorporate Roe’s approximate Riemann solver [20] in [21]. Hillman et al. [22] investigated nodally integrated RKPM with the SUPG stabilization and employed the concept of implicit gradient approximation [23] to embed stabilization into the gradient of test functions without explicit differentiation. This approach is further elaborated by Huang [24], in which a variationally consistent SUPG meshfree approach was developed.

Recently, there has been growing interest in strong form-based collocation methods, which involve directly solving PDEs by discretizing field variables in recent years. Developing high-order approximation techniques such as meshfree methods has made this approach possible. Meshfree approximations, known for their high-order smoothing and compatible shape functions, are particularly well-suited for strong form collocation methods. This makes them an ideal choice, especially when dealing with high-order approximations—an aspect traditionally challenging for element-based  $C^0$  type finite element approximation [25–28]. The node-based collocation methods are an attractive option for solving PDEs because they do not require numerical integration, which improves computational efficiency and simplifies the method. Since the non-self-adjoint nature of convection-diffusion problems, the common intuition is to employ the Petrov-Galerkin numerical approaches for stabilization. While Petrov-Galerkin methods effectively stabilize issues with strong convection effects, direct collocation methods, a subset of Petrov-Galerkin, employing a Dirac delta test function, exhibit instability when directly applied to convection-dominated problems. To ensure stability, an upwind treatment for the convection terms becomes essential.

This work will systematically develop a consistent stabilized meshfree collocation framework, particularly emphasizing the convection-dominated problems. The framework is initialized by connecting the finite difference scheme and the gradient smoothing technique [10] in meshfree methods. The upwind finite difference approximation is identified as equivalent to applying gradient smoothing over the upwind side of the nodal representative domain. It is then revealed that the upwind treatment of the first-order gradient term is akin to evaluating the point over the upwind side of the nodal representative domain. The selection of evaluation points of the upwind collocation method is justified by the 1D FEM recursive gradient. Following this, the upwind collocation methodology is extended to the reproducing kernel collocation method within a pure meshfree setting. The error analysis shows that the proposed upwind reproducing kernel collocation method can achieve at least  $(p - 1)$ th order convergence rate, where  $p$  is the order of basis function in reproducing kernel approximation. The essence of the present work is to treat the first-order convection term by properly selecting the collocation points according to the flow direction and Péclet number. The upwind effect is achieved without introducing artificial parameters, and its application to multi-dimensional and transient cases is straightforward. The current collocation framework exhibits no cross-wind diffusion. Furthermore, we establish that consistently collocating the governing equations is essential for achieving optimal convergence rate and accuracy. This contrasts with many early-developed upwind approaches that focus solely on the treatment of the first-order convection term. The effectiveness of the proposed algorithm is well demonstrated through a series of steady and unsteady numerical examples.

The remainder of this paper is as follows. Section 2 reviews the basic formulation of convection-diffusion problems, Bubnov-Galerkin and collocation schemes, and the numerical instability arising from those standard methods. The upwind collocation technique is then introduced in Section 3, where the selection of collocation location is explained by employing the distinct 1D recursive FEM shape function. The upwind collocation method is then extended to the reproducing kernel particle method framework in Section 4 with detailed error analysis. In Section 5, several 1D and 2D numerical examples are provided to show the effectiveness of the proposed method in both steady and transient problems, which is finally followed by concluding remarks in Section 6.

## 2 Model problem

### 2.1 Bubnov-Galerkin approach for convection-diffusion equation

The multi-dimensional convection-diffusion problem is considered the model problem in this work:

$$\begin{aligned} \mathbf{a} \cdot \nabla u &= k\Delta u + s & \mathbf{x} \in \Omega \\ k\nabla u \cdot \mathbf{n} &= \bar{h} & \mathbf{x} \in \Gamma_h, \\ u &= u_g & \mathbf{x} \in \Gamma_g \end{aligned} \quad (1)$$

where  $\mathbf{a} = \{v_x, v_y\}$  is the convection velocity vector,  $k$  is the diffusivity,  $s$  is the source term,  $u$  is the displacement or potential. The constant diffusivity  $k$  is considered in the present work.  $\Gamma_g$  is the essential boundary of the problem domain  $\Omega$  with the prescribed value  $u_g$ .  $\Gamma_h$  is the diffusive-type boundary with flux  $\bar{h}$ .

The traditional weak form of Eq. (1) is to find  $u \in U$  such that for all  $w \in W$  the following holds:

$$a(w, u)_\Omega = (w, s)_\Omega + (w, \bar{h})_{\Gamma_h}, \quad (2)$$

where  $U$  and  $W$  are Sobolev spaces of degree one under properly satisfied essential boundary conditions,  $(\cdot, \cdot)_\Omega$  and  $(\cdot, \cdot)_{\Gamma_h}$  represent the  $L_2$  inner product over the domain and Neumann boundary. In this work, we consider the diffusion-type Neumann boundary condition. Furthermore, the bilinear form  $a(\cdot, \cdot)$  reads as follows:

$$a(w, u)_\Omega = (k\nabla w, \nabla u)_\Omega + (w, \mathbf{a} \cdot \nabla u)_\Omega. \quad (3)$$

The Bubnov-Galerkin weak form considers the subspaces  $U^h \subset U$  and  $W^h \subset W$  and find  $u^h \in U^h$  such that for all  $w^h \in W^h$  the following holds:

$$a(w^h, u^h)_\Omega = (w^h, s)_\Omega + (w^h, \bar{h})_{\Gamma_h}. \quad (4)$$

The matrix version of Eq. (4) is obtained through the approximation of field variable  $u^h(\mathbf{x}) = \sum_{I=1}^{NP} N_I(\mathbf{x})u_I$ :

$$\mathbf{K}\mathbf{u} = \mathbf{f}, \quad (5)$$

where  $\mathbf{u}$  is the column vectors of  $\{u_I\}_{I=1}^{NP}$ ,  $N_I(\mathbf{x})$  is the shape function associated with  $I$ th node,  $NP$  denotes the total number of nodes in the discretization,  $\mathbf{K}$  and  $\mathbf{f}$  are so-called stiffness matrix and force vectors, respectively:

$$K_{IJ} = \int_{\Omega} N_I \mathbf{a} \cdot \nabla N_J + \nabla N_I \cdot k \nabla N_J \, d\Omega, \quad (6)$$

$$f_I = \int_{\Omega} N_I s \, d\Omega + \int_{\Gamma_h} N_I \bar{h} \, d\Gamma. \quad (7)$$

The Dirichlet boundary condition in Eq. (6) can be enforced by employing static condensation [1]. As can be observed from Eq. (6), since the existence of convection term, the stiffness matrix does not preserve the symmetricity under the Bubnov-Galerkin setting, i.e.  $\mathbf{K} \neq \mathbf{K}^T$ . Numerical instability is thus arrived due to this feature, which will be introduced in the following section. A detailed illustration of building the shape functions will be presented in Section 4.

### 2.2 Point collocation approach for convection-diffusion equation

An alternative numerical approach for solving partial differential equations lies in the Petrov-Galerkin [1] setting. The point collocation method, which considers the evaluation of the governing equation and boundary conditions at several collocation points in the domain and boundaries, belongs to the scope of the Petrov-Galerkin approach. Although in this method, the selection of collocation points is arbitrary, it is evident that choosing those as nodal points to be the collocation points is simplest and can achieve optimal convergence rate [27]. The related formulation statement is given as:

$$\begin{aligned} \mathbf{a}(\mathbf{x}_I) \cdot \nabla u(\mathbf{x}_I) &= k\Delta u(\mathbf{x}_I) + s(\mathbf{x}_I), & \mathbf{x}_I \in \Omega \\ k\nabla u(\mathbf{x}_I) \cdot \mathbf{n} &= \bar{h}(\mathbf{x}_I), & \mathbf{x}_I \in \Gamma_h, \\ u(\mathbf{x}_I) &= u_g(\mathbf{x}_I), & \mathbf{x}_I \in \Gamma_g \end{aligned} \quad (8)$$

where  $\mathbf{x}_I$  denotes the location collocation points. The first row of Eq. (8) denotes that an evaluation point in the interior domain is subjecting the governing equation. The second row corresponds to the collocation points located at the Neumann boundary. Finally, the last row represents the Dirichlet boundary condition.

Substituting the approximation of field variable directly into Eq. (8) leads to the following discrete collocation system of equations:

$$\mathbf{K}^C \mathbf{u} = \mathbf{f}^C, \quad (9)$$

where the entries of the matrices and force vector are given by:

$$K_{IJ}^C = \begin{cases} \mathbf{a}(\mathbf{x}_I) \cdot \nabla N_J(\mathbf{x}_I) - k\Delta N_J(\mathbf{x}_I), & \mathbf{x}_I \in \Omega \\ \mathbf{n} \cdot k\nabla N_J(\mathbf{x}_I), & \mathbf{x}_I \in \Gamma_h \\ N_J(\mathbf{x}_I), & \mathbf{x}_I \in \Gamma_g \end{cases}, \quad (10)$$

$$f_I^C = \begin{cases} s(\mathbf{x}_I), & \mathbf{x}_I \in \Omega \\ \bar{h}(\mathbf{x}_I), & \mathbf{x}_I \in \Gamma_h \\ \bar{u}_g(\mathbf{x}_I), & \mathbf{x}_I \in \Gamma_g \end{cases}. \quad (11)$$

In contrast to the previous Bubnov-Galerkin weak form, the strong form collocation scheme requires higher order continuous shape function as required by the direct approximation on the diffusion term. The  $C^1$  continuous shape function is not easy to build in the traditional approach but is favorable in some advanced numerical techniques, e.g., meshfree, and IGA [29]. As noticed from (10), the stiffness matrix in such a system is intrinsically non-symmetric as it employs the Dirac function as the test function.

### 2.3 Instability in solving non-self-adjoint problem with Bubnov-Galerkin and collocation methods

In general, the solution to (1) exhibits diffusion dominated when the Péclet number  $Pe = \|a\|L/k$  becomes insignificant. However, as the convection effect becomes intense, the high Péclet number leads to boundary layers, and numerical instability will be observed when considering the traditional Bubnov-Galerkin approaches. When a 1D version of Eq. (1) is considered without the contribution from the source term, the general solution is given as follows:

$$u(x) = C_1 + C_2 e^{\frac{v}{k}x}, \quad (12)$$

where  $C_1$  and  $C_2$  are arbitrary constants corresponding to the boundary conditions. Meanwhile, apply traditional finite element or finite difference schemes apply to (1) without the source term, the numerical solution associated with the  $I - th$  interior node is given as [30]:

$$u_I = C_1 + C_2 \left( \frac{1 + Pe^h}{1 - Pe^h} \right)^I, \quad (13)$$

where the element Péclet number is defined as  $Pe^h := vh/(2k)$  and  $h$  denotes the element size. Comparing Eq. (13) with (12), the numerical will exhibit oscillation for the case when  $Pe^h > 1$ . To demonstrate this, the comparison of the 1D convection-diffusion problem is provided in Fig. 1 with the boundary condition  $u(0) = 0$  and  $u(1) = 1$ . No source term is considered in this case. Three numerical approaches have been employed in this comparison. The finite element method (FEM) and reproducing kernel particle method (RKPM) are two representative numerical methods under the Bubnov-Galerkin setting. The reproducing kernel collocation method (RKCM) is also added to this comparison as a representative Petrov-Galerkin method. The element Péclet number is chosen as  $Pe^h = 2.5$ , and severe oscillations are noticed from both FEM, RKPM, and RKCM.

**Remark 1.** *Although the collocation method is considered a Petrov-Galerkin approach, numerical oscillation is still observed when applying it to convection-dominated problems. It is well acknowledged that by properly designing the test function, the Petrov-Galerkin approach serves as a numerical remedy to the instability. This motivates our present work to systematically develop the collocation method for the convection-dominated problems.*

## 3 Upwind collocation method for convection-dominated problems

The upwind treatment for the convection term can be considered a remedy for this instability. The idea of the upwind scheme is to select different approximations particular for the convection term to enable consistent behavior between the numerical solution and the exact solution.

### 3.1 Finite difference and an alternative interpretation

#### 3.1.1 Central difference

In the traditional finite element or finite difference methods, the approximation for the first order derivative of the field variable, denoted by  $u_{,x}^h$ , is given as:

$$u_{,x}^h(x_I) = \frac{u_{I+1} - u_{I-1}}{2h}, \quad (14)$$



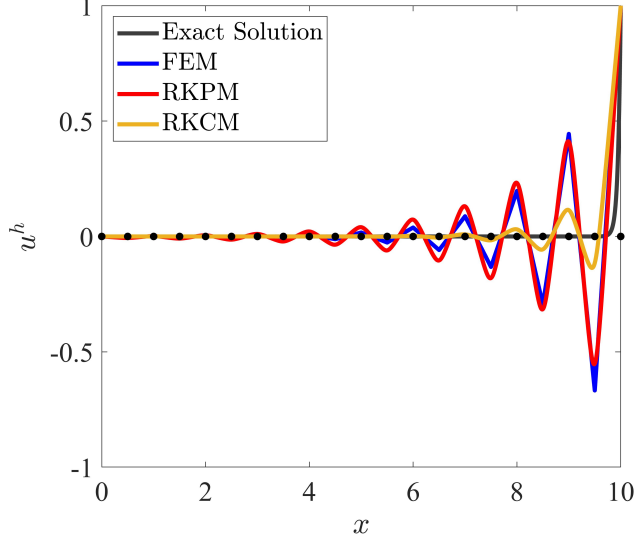


Figure 1: Oscillatory behavior in FEM, RKPM, and collocation applied to the convection-diffusion equation with element Péclet number  $Pe^h = 2.5$ .

which is so-called the central difference approximation. The related stencils of the central difference scheme are given as

$$\left. \frac{du}{dx} \right|_{x_I} \sim \frac{1}{2h}(-1, 0, 1) = \frac{1}{h}(0, 0.5, 0.5) - \frac{1}{h}(0.5, 0.5, 0). \quad (15)$$

The motivation for the last step in (15) is to relate the stencils to the evaluation of shape function at the specific points. For the central difference scheme, the approximation of the first-order derivative of the field variable is rephrased as:

$$\begin{aligned} u_{,x}^h(x_I) &= \frac{1}{h} (\{0, 0.5, 0.5\} - \{0.5, 0.5, 0\}) \{u_{I-1}, u_I, u_{I+1}\}^T \\ &= \frac{1}{h} \left[ \mathbf{N}^{\text{FEM}} \left( \frac{x_I + x_{I+1}}{2} \right) - \mathbf{N}^{\text{FEM}} \left( \frac{x_{I-1} + x_I}{2} \right) \right] \mathbf{u}, \end{aligned} \quad (16)$$

where  $\mathbf{N}^{\text{FEM}}(x)$  is a vector containing all the 1D finite shape functions evaluated at a spatial point. More specifically, due to the existence of the compact support for the shape function, in this case,  $\mathbf{N}^{\text{FEM}}(x) = \{N_{I-1}^{\text{FEM}}(x), N_I^{\text{FEM}}(x), N_{I+1}^{\text{FEM}}(x)\}$ . As shown in Fig. 2 (a), the central difference is equivalent to taking the difference of the shape function vector evaluated at the center of downwind and upwind elements of point  $x_I$ . By imposing the first fundamental theorem of calculus, the central difference approximation of the first-order derivative of the field variable has been transferred to an integral-type approach:

$$u_{,x}^h(x_I) = \frac{1}{h} \int_{(x_{I-1}+x_I)/2}^{(x_I+x_{I+1})/2} \mathbf{N}_{,x}^{\text{FEM}}(x) dx \mathbf{u} := \int_{\Omega} \psi(x; x - x_I) \mathbf{N}_{,x}^{\text{FEM}}(x) dx \mathbf{u}, \quad (17)$$

where  $\psi(x; x - x_I)$  is the Heaviside function:

$$\psi(x; x - x_I) = \begin{cases} 1/h & x \in \left[ \frac{x_{I-1}+x_I}{2}, \frac{x_I+x_{I+1}}{2} \right] \\ 0 & \text{else} \end{cases}. \quad (18)$$

From Eq. (16), we observe that the central difference approximation of the first order derivative of the field variable in Eq. (17) is identical to the well-known strain smoothing technique introduced in the scope of meshfree methods by Chen et. al. [10].

### 3.1.2 Upwind difference

When a positive velocity  $v$  is considered in the 1D problem, the solution can be interpreted as a traveling wave propagating towards the right side. The left side of the domain is called the upwind side, whereas the right side is the downwind side. Then the upwind approximation of field variable, denoted by  $\tilde{u}_{,x}^h$ , reads as:

$$\tilde{u}_{,x}^h(x_I) = \frac{u_I - u_{I-1}}{h}, \quad (19)$$

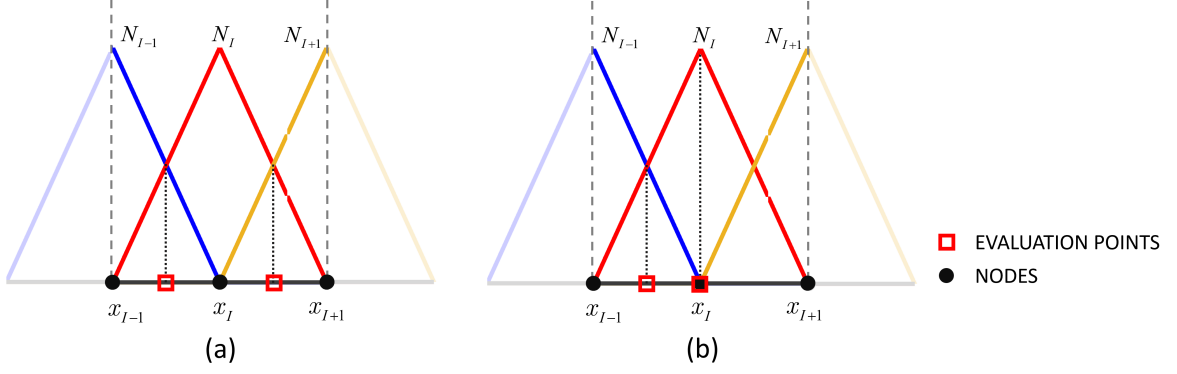


Figure 2: Interpretation of finite difference stencils: (a) central difference stencils; (b) upwind difference stencils,  $v(x_I) > 0$ .

which can be interpreted as employing the first-order difference scheme to the convection term with the aid of the upwind side point. The related stencils of the upwind difference scheme are given by:

$$\left. \frac{d\tilde{u}}{dx} \right|_{x_I} \sim \frac{1}{h}(-1, 1, 0) = \frac{1}{h/2}(0, 1, 0) - \frac{1}{h/2}(0.5, 0.5, 0). \quad (20)$$

Similarly, from Fig. 2(b), it is evident that the upwind approximation in (20) can be rephrased as:

$$\begin{aligned} \tilde{u}_{,x}^h(x_I) &= \frac{1}{h/2} (\{0, 1, 0\} - \{0.5, 0.5, 0\}) \mathbf{u} \\ &= \frac{1}{h/2} \left[ \mathbf{N}^{\text{FEM}}(x_I) - \mathbf{N}^{\text{FEM}}\left(\frac{x_{I-1} + x_I}{2}\right) \right] \mathbf{u} \\ &= \frac{1}{h/2} \int_{(x_{I-1} + x_I)/2}^{x_I} \mathbf{N}_{,x}^{\text{FEM}}(x) dx \mathbf{u} := \int_{\Omega} \bar{\psi}(x; x - x_I) \mathbf{N}_{,x}^{\text{FEM}}(x) dx \mathbf{u}, \end{aligned} \quad (21)$$

where the convolution function is defined as:

$$\bar{\psi}(x; x - x_I) = \begin{cases} \psi^-(x; x - x_I), & v(\mathbf{x}_I) > 0 \\ \psi^+(x; x - x_I), & v(\mathbf{x}_I) < 0 \end{cases}, \quad (22)$$

and for different directions, the convolution functions are given as:

$$\psi^-(x; x - x_I) = \begin{cases} 1/(h/2), & x \in \left[ \frac{x_{I-1} + x_I}{2}, x_I \right] \\ 0, & \text{else} \end{cases}, \quad (23)$$

$$\psi^+(x; x - x_I) = \begin{cases} 0, & \text{else} \\ 1/(h/2), & x \in \left[ x_I, \frac{x_I + x_{I+1}}{2} \right] \end{cases}. \quad (24)$$

Consistently with the central difference scheme, the upwind approximation can also be interpreted as taking the gradient smoothing of the shape function over the domain. Nevertheless, the domain of the convolution integral is on the upwind side of the nodal representative region, which is no longer centered at the point of interest.

Finally, the upwind finite difference approximation for the first-order term has successfully been interpreted as gradient smoothing in solid mechanics.

### 3.2 Upwind collocation method

Although the discovery of the upwind scheme with gradient smoothing in Eq. (21) is under the 1D assumption, one can also generate the concept to the multi-dimensional case. First, the central difference representation in the multi-dimensional case is:

$$\nabla u^h(\mathbf{x}_I) = \int_{\Omega} \psi(\mathbf{x}; \mathbf{x} - \mathbf{x}_I) \nabla \mathbf{N}(\mathbf{x}) d\Omega \mathbf{u}, \quad (25)$$

where

$$\psi(\mathbf{x}; \mathbf{x} - \mathbf{x}_I) = \begin{cases} 1/V_I, & \mathbf{x} \in \Omega_I \\ 0, & \mathbf{x} \notin \Omega_I \end{cases}, \quad (26)$$

where  $\Omega_I$  is the representative domain of node  $\mathbf{x}_I$  as shown in Figure 3(a) obtained from Voronoi diagram with  $V_I$  being the volume of the representative domain  $\Omega_I$ . In the original work of gradient smoothing [10], the authors considered the convolution operation on the right-hand side of Eq (25) serving as an alternative approximation of the gradient of field variation at  $\mathbf{x}_I$  providing the shape function has high order smoothness, i.e.

$$\nabla u^h(\mathbf{x}_I) = \nabla \mathbf{N}(\mathbf{x}_I) \mathbf{u} \approx \left( \frac{1}{V_I} \int_{\Omega_I} \nabla \mathbf{N}(\mathbf{x}) \, d\Omega \right) \mathbf{u}. \quad (27)$$

If carrying out one point quadrature of the right-hand side with  $\mathbf{x}_I$  being the evaluation point, one immediately has:

$$\left( \frac{1}{V_I} \int_{\Omega_I} \nabla \mathbf{N}(\mathbf{x}) \, d\Omega \right) \mathbf{u} \approx \left( \frac{1}{V_I} \widehat{\int}_{\Omega_I} \nabla \mathbf{N}(\mathbf{x}) \, d\Omega \right) \mathbf{u} = \frac{1}{V_I} \{V_I \nabla \mathbf{N}(\mathbf{x}_I)\} \mathbf{u} = \nabla u^h(\mathbf{x}_I), \quad (28)$$

where  $\widehat{\int}_{\Omega_I} \square \, d\Omega$  denotes the numerical version of integration. From Eq. (27) to Eq. (28), it is clear that the smoothed gradient over  $\Omega_I$  can be treated as the approximation of the first order gradient of the field variable. However, the numerical integration to the smoothed gradient can be performed arbitrarily. Different selections of evaluation points for the quadrature may finally yield different approximations of the field variable as indicated from Eq. (28).

Similar to the 1D case, the upwind approximation for the gradient of the field variable in the multi-dimensional case is given as:

$$\nabla \tilde{u}(\mathbf{x}_I) = \int_{\Omega} \tilde{\psi}(\mathbf{x}; \mathbf{x} - \mathbf{x}_I) \nabla \mathbf{N}(\mathbf{x}) \, d\Omega \mathbf{u}, \quad (29)$$

where:

$$\tilde{\psi}(\mathbf{x}; \mathbf{x} - \mathbf{x}_I) = \begin{cases} 1/\tilde{V}_I, & \mathbf{x} \in \tilde{\Omega}_I \\ 0, & \mathbf{x} \notin \tilde{\Omega}_I. \end{cases} \quad (30)$$

In the upwind convolution operation, as illustrated in Figure 3 (b) and (c),  $\tilde{\Omega}_I = \{\mathbf{x} \in \Omega_I | (\mathbf{x} - \mathbf{x}_I) \cdot \mathbf{n} \leq 0\}$ ,  $\mathbf{n}(\mathbf{x}_I) = \mathbf{a}(\mathbf{x}_I)/\|\mathbf{a}(\mathbf{x}_I)\|$  is the normalized flow speed vector and  $\tilde{V}_I$  denotes the volume of upwind smoothing domain. Creating the upwind smoothing domain involves finding the plane perpendicular to the flow direction, which contains the particle  $\mathbf{x}_I$ . After finding the plane, the smoothing zone is the upwind side of the representative domain.

Once the upwind treatment of the first-order term is set up, the next important step is to carry out the quadrature for the upwind smoothed gradient. The approximated version of Eq. (29) is obtained by performing the simplest one-point quadrature in the upwind domain:

$$\nabla \tilde{u}(\mathbf{x}_I) = \frac{1}{\tilde{V}_I} \int_{\tilde{\Omega}_I} \nabla \mathbf{N}(\mathbf{x}) \, d\Omega \mathbf{u} \approx \frac{1}{\tilde{V}_I} \widehat{\int}_{\tilde{\Omega}_I} \nabla \mathbf{N}(\mathbf{x}) \, d\Omega \mathbf{u} = \frac{1}{\tilde{V}_I} (\tilde{V}_I \nabla \mathbf{N}(\mathbf{x}_C)) \mathbf{u} = \nabla u(\mathbf{x}_C), \quad (31)$$

where  $\mathbf{x}_C$  serves as the upwind collocation point for stabilizing the strong convection term. Finally, the most important concept of this research work is introduced from Eq. (31). The upwind stabilization to the convection-dominated problems is equivalent to evaluating the convection term within the upwind side of the particle. Consequently, the upwind collocation formulation is given by modifying the traditional collocation method in Eq. (8) as follows:

$$\begin{aligned} \mathbf{a}(\mathbf{x}_C) \cdot \nabla u(\mathbf{x}_C) &= k \Delta u(\mathbf{x}_C) + s(\mathbf{x}_C), & \mathbf{x}_C \in \mathcal{C}_I \subseteq \tilde{\Omega}_I \\ k \nabla u(\mathbf{x}_I) \cdot \mathbf{n} &= \tilde{h}(\mathbf{x}_I), & \mathbf{x}_I \in \Gamma_h \\ u(\mathbf{x}_I) &= u_g(\mathbf{x}_I), & \mathbf{x}_I \in \Gamma_g \end{aligned} \quad (32)$$

where  $\mathcal{C}_I = \{\mathbf{x} \in \tilde{\Omega}_I | (\mathbf{x} - \mathbf{x}_I) \cdot \mathbf{n} + \|\mathbf{x} - \mathbf{x}_I\| = 0\}$  is the line formed by the reverse extension of flow direction  $\mathbf{n}$ .

In the upwind collocation formula (32), the essential idea is to have the convection term treated in a stabilized way when the problem is convection-dominated. A similar idea had been proposed in literature [31], which evaluated the convection term differently than diffusion and source terms in the weak form setting to achieve the upwind stabilization in a FEM way. Nevertheless, numerical inconsistency has been observed [3] in those upwind finite element methods, and especially for the pure convection problem with source term, the traditional upwind treatment does not yield good performance compared to the central difference schemes. In fact, although only the convection response is properly treated, the remaining diffusion and source terms are not modified correspondingly. In the present formulation (32), the upwind collocation formula considered the governing equation being evaluated at the same location  $\mathbf{x}_C$ , which achieves the desired consistency. The importance of consistency will be further addressed by error analysis in Section 4 and demonstrated through the numerical examples in Section 5.

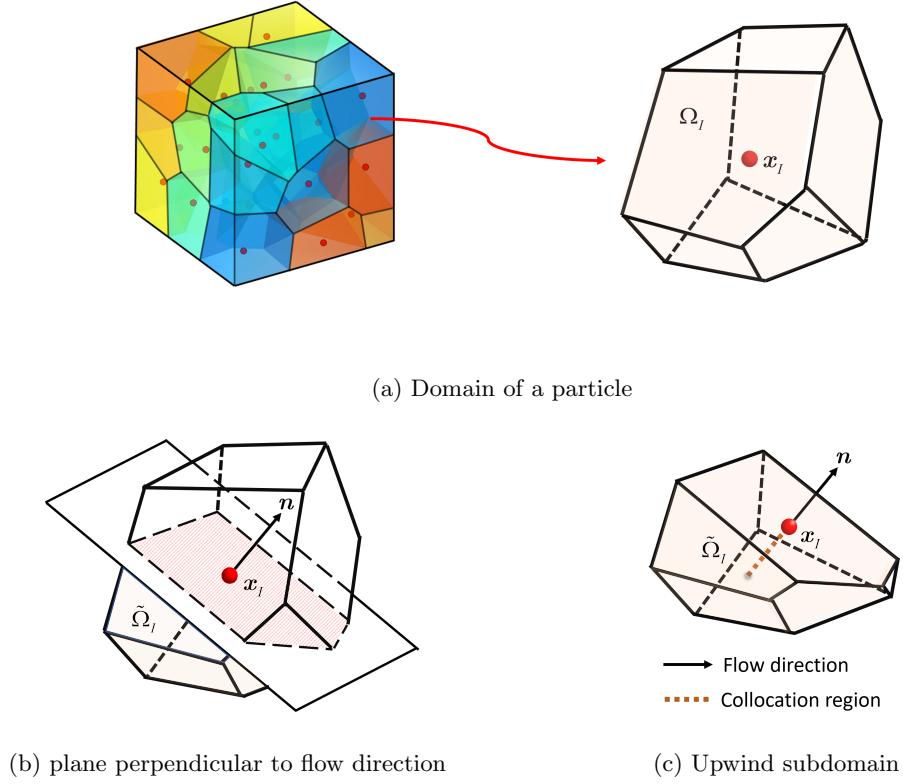


Figure 3: Representative domain of a particle  $x_I$

### 3.3 Selection of upwind collocation points

After formulating the upwind collocation method, the selection of the detailed location of upwind points will be introduced since the previous section only defines the collocation point  $x_C$  as the neighborhood of  $x_I$ . In the present work, to achieve the best accuracy, the selection of collocation points  $x_C$  is based on the intensity of convection. By substituting the approximation of the field variable, the collocation equation with respect to the interior evaluation points in Eq. (32) becomes:

$$vu_{,x}^h(x_C) - ku_{,xx}^h(x_C) = v \sum_J N_{J,x}(x_C) u_J - k \sum_J N_{J,xx}(x_C) u_J = 0, \quad (33)$$

where the source term is not considered. To express  $x_C$  in terms of nodal space, diffusivity, and/or convection speed, the following assumptions are made for the subsequent derivation in this section:

- The particles are under uniform discretization with the same nodal distance  $h$ .
- $x_I$  is the closest node to the collocation point  $x_C$ .
- $N_I$  is at least  $C^1$  continuous shape function and  $x_C$  is not evaluated on the location where the second order derivative of  $N_I$  does not exist.
- $x_C$  is covered by maximum 3 neighboring shape functions  $N_{I-1}(x)$ ,  $N_I(x)$ , and  $N_{I+1}(x)$ .
- The shape function used in approximation satisfies at least partition of unity and linear completeness, i.e.  $\sum_J N_J(x) = 1$  and  $\sum_J N_J(x)x_J = x$ .

With the aid of the first assumption i.e., uniform distribution  $x_J = Jh$  and  $u(x_J) = u_J$ , Eq. (33) becomes to:

$$C_1 \left( v \sum_J N_{J,x}(x_C) - k \sum_J N_{J,xx}(x_C) \right) + C_2 \left( v \sum_J N_{J,x}(x_C) e^{\frac{vh}{k}J} - k \sum_J N_{J,xx}(x_C) e^{\frac{vh}{k}J} \right) = 0. \quad (34)$$

Define  $\lambda = e^{vh/k}$  and by utilizing the partition of unity of shape function, one immediately gets the following from Eq. (34):

$$v \sum_J N_{J,x}(x_C) \lambda^J - k \sum_J N_{J,xx}(x_C) \lambda^J = 0. \quad (35)$$

Introducing the third assumption that  $x_C$  is covered by maximum 3 neighboring points, Eq. (35) can be written in the explicit form:

$$\left(\frac{v}{k}N_{I-1,x}(x_C) - N_{I-1,xx}(x_C)\right)\lambda^{I-1} + \left(\frac{v}{k}N_{I,x}(x_C) - N_{I,xx}(x_C)\right)\lambda^I + \left(\frac{v}{k}N_{I+1,x}(x_C) - N_{I+1,xx}(x_C)\right)\lambda^{I+1} = 0. \quad (36)$$

Then, it is easy to compute the non-zero roots of Eq. (36), which are:

$$\lambda_1 = 1, \quad \lambda_2 = \frac{N_{I-1,xx}(x_C) - \frac{v}{k}N_{I-1,x}(x_C)}{N_{I+1,xx}(x_C) - \frac{v}{k}N_{I+1,x}(x_C)}. \quad (37)$$

Finally, the numerical solution of  $u_I$  in terms of the shape function is expressed as follows:

$$u_I = C_1\lambda_1^I + C_2\lambda_2^I = C_1 + C_2 \left(\frac{N_{I-1,xx}(x_C) - \frac{v}{k}N_{I-1,x}(x_C)}{N_{I+1,xx}(x_C) - \frac{v}{k}N_{I+1,x}(x_C)}\right)^I. \quad (38)$$

Compare the numerical solution in Eq. (38) with the exact solution in Eq. (12), and the following statement should hold for the best accuracy and consistency:

$$e^{vh/k} = \frac{N_{I-1,xx}(x_C) - \frac{v}{k}N_{I-1,x}(x_C)}{N_{I+1,xx}(x_C) - \frac{v}{k}N_{I+1,x}(x_C)}. \quad (39)$$

The relationship between the location of collocation points  $x_C$ , and the flow velocity is connected in Eq. (39) in an implicit way. Once the explicit form of the shape function is provided, the collocation point can be directly connected to the element Péclet number.

In order to provide a general strategy for selecting collocation points, the partition of unity and linear completeness of shape function is invoked:

$$\sum_J N_J(x) = 1, \quad \sum_J N_J(x) x_J = x. \quad (40)$$

The variants of Eq. (40) hold under the uniform distribution assumption:

$$N_{I+1,x}(x_C) = \frac{1}{h} + N_{I-1,x}(x_C), \quad N_{I+1,xx}(x_C) = N_{I-1,xx}(x_C). \quad (41)$$

By substituting Eq. (41) back to Eq. (39), one has:

$$\frac{h^2}{2}N_{I-1,xx}(x_C) - Pe^h h N_{I-1,x}(x_C) = \frac{Pe^h}{e^{2Pe^h} - 1} + Pe^h. \quad (42)$$

An implicit relationship between the collocation points  $x_C$  and element Péclet number  $Pe^h$  was built by Eq. (42). Furthermore, different shape functions may yield different relationships for  $x_C$  and  $Pe^h$ , i.e. the IGA shape function [29] built with splines and the RKPM shape function [14], which is a rational function.

### 3.3.1 Design an explicit relationship between collocation points and element Péclet number by design a $C^1$ polynomial shape function

To generate an explicit expression, the goal is to define a shape function where the second-order derivatives are piecewise constant in space and the first-order derivative is linear. Nevertheless, the traditional FEM shape function has only a piecewise constant in its first-order derivative, which is not feasible for locating  $x_C$ . The concept of recursive gradient [28] provides an alternative way to build high order smoothed gradient of the shape function by using the lower order derivatives. First, the 1D FEM linear shape function, denoted by  $N_I^{\text{FEM}}(x)$  reads as:

$$N_I^{\text{FEM}}(x) = \begin{cases} 0, & x \leq x_{I-1} \\ (x - x_{I-1}) / (x_I - x_{I-1}), & x_{I-1} < x \leq x_I \\ (x_{I+1} - x) / (x_{I+1} - x_I), & x_I < x < x_{I+1} \\ 0, & x_{I+1} \leq x \end{cases}. \quad (43)$$

The recursive first-order FEM gradient of the shape function is computed by interpolating some sampling first-order FEM gradient data with the FEM shape function itself:

$$\tilde{N}_{I,x}(x) = N_{J_1}^{\text{FEM}}(x)N_{I,x}^{\text{FEM}}(x_{J_1}) + N_{J_2}^{\text{FEM}}(x)N_{I,x}^{\text{FEM}}(x_{J_2}) = \frac{1}{h}(N_{J_1}^{\text{FEM}}(x) - N_{J_2}^{\text{FEM}}(x)), \quad (44)$$

where  $x_{J_1} \in (x_{I-1}, x_I)$  and  $x_{J_2} \in (x_I, x_{I+1})$  are some sampling points. Eq. (44) can also be viewed as taking the central difference of two finite element shape functions. Next question is how to build  $N_{J_1}(x)$  and  $N_{J_2}(x)$ . In this work, the most straightforward case is selected i.e.  $x_{J_1}$  and  $x_{J_2}$  are at the center of each element:

$$x_{J_1} = (x_{I-1} + x_I)/2, \quad x_{J_2} = (x_I + x_{I+1})/2. \quad (45)$$

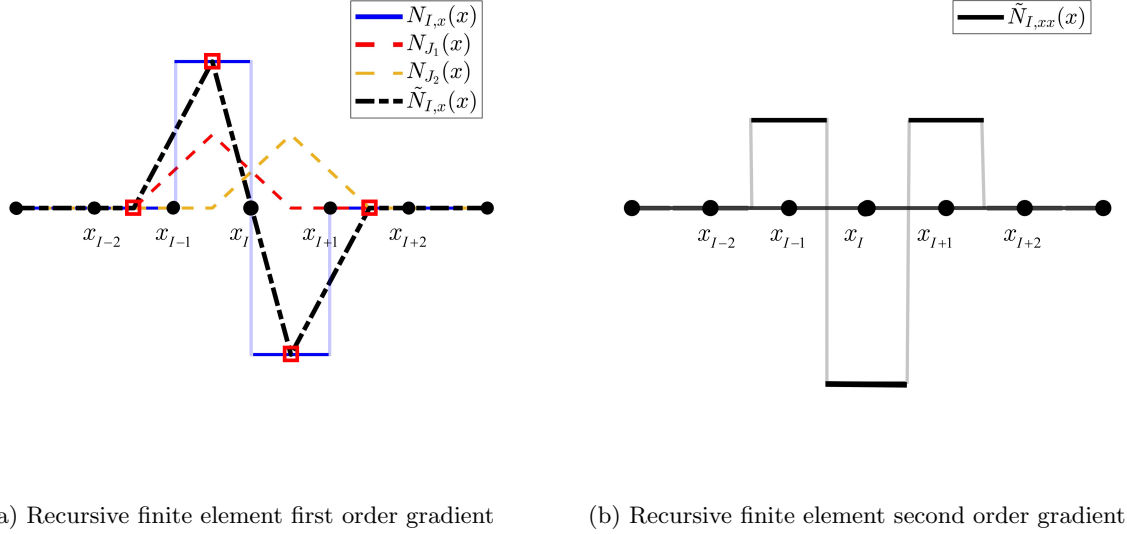


Figure 4: Recursive finite element gradients.

Meanwhile, the element shape function is built under the same element size  $h$  with the node located at the center of each element. A detailed illustration of this recursive FEM gradient is provided in Figure 4. Finally, the explicit form of 1D recursive FEM first order gradient of function states as:

$$\tilde{N}_{I,x}(x) = \frac{1}{h^2} \begin{cases} 0, & x \leq \frac{x_{I-2}+x_{I-1}}{2} \\ \left(x - \frac{x_{I-2}+x_{I-1}}{2}\right), & \frac{x_{I-2}+x_{I-1}}{2} < x \leq \frac{x_{I-1}+x_I}{2} \\ 2(x_I - x), & \frac{x_{I-1}+x_I}{2} < x \leq \frac{x_I+x_{I+1}}{2} \\ \left(x - \frac{x_{I+1}+x_{I+2}}{2}\right), & \frac{x_I+x_{I+1}}{2} < x \leq \frac{x_{I+1}+x_{I+2}}{2} \\ 0, & x > \frac{x_{I+1}+x_{I+2}}{2} \end{cases}. \quad (46)$$

The second-order gradient is given by directly differentiating:

$$\tilde{N}_{I,xx}(x) = \frac{1}{h^2} \begin{cases} 0, & x < \frac{x_{I-2}+x_{I-1}}{2} \\ 1, & \frac{x_{I-2}+x_{I-1}}{2} < x < \frac{x_{I-1}+x_I}{2} \\ -2, & \frac{x_{I-1}+x_I}{2} < x < \frac{x_I+x_{I+1}}{2} \\ 1, & \frac{x_I+x_{I+1}}{2} < x < \frac{x_{I+1}+x_{I+2}}{2} \\ 0, & x > \frac{x_{I+1}+x_{I+2}}{2} \end{cases}. \quad (47)$$

We should notice that with the operation, the shape function derivative passing the nodal point is continuous. The jump happened in the mid of each element, which is acceptable in the point collocation approach. It is easy to show that the recursive first and second-order FEM gradient satisfy the partition of unity and linear completeness properties [27], which are the key requirement in determining the collocation point. Now since  $x_C \in [\frac{x_{I-1}+x_I}{2}, \frac{x_I+x_{I+1}}{2}]$  is the point in the representative domain of  $x_I$ , the  $(I-1)$ th recursive FEM gradient evaluated at  $x_C$  reads as follows:

$$\tilde{N}_{I-1,x}(x_C) = \frac{2x_C - (x_I + x_{I+1})}{2h^2}, \quad \tilde{N}_{I-1,xx}(x_C) = \frac{1}{h^2}. \quad (48)$$

Finally, substitute Eq. (48) back to Eq. (42), one has:

$$\xi = \coth\left(Pe^h\right) - \frac{1}{Pe^h}, \quad (49)$$

where  $\xi = (x_I - x_C)/(h/2)$  is the normalized collocation distance. As  $x_C \in [\frac{x_{I-1}+x_I}{2}, \frac{x_I+x_{I+1}}{2}]$ , the corresponding range of  $\xi$  will be  $[-1, 1]$ . In the meantime, when  $\xi \in [-1, 1]$ , it automatically defines the domain of  $Pe^h \in [-\infty, \infty]$  from right hand side of Eq. (49). The following special cases for  $\xi$  are:

$$\xi = \begin{cases} 0, & Pe^h = 0 \\ \pm 1, & Pe^h = \pm\infty \end{cases} \Rightarrow \begin{cases} \text{pure diffusion} \\ \text{pure convection} \end{cases}, \quad (50)$$

where the corresponding  $x_C$  becomes:

$$x_C = \begin{cases} x_I, & Pe^h = 0 \\ \frac{1}{2}(x_I + x_{I\mp 1}), & Pe^h = \pm\infty \end{cases} \Rightarrow \begin{cases} \text{pure diffusion} \\ \text{pure convection} \end{cases}. \quad (51)$$

From Eq. (49), the location of the upwind collocation point is connected to the element Péclet number. In the final conclusion (51), as the Péclet number goes to 0, corresponding to the pure diffusion problem, then the collocation point is chosen to be the same as the nodal position. When the Péclet number goes to infinity, the collocation point is suggested as the boundary of the representative upwind domain of the particle.

**Remark 2.** *The hyperbolic type function on the right-hand side of Eq. (49) is well acknowledged in the literature as a stabilization measure used to control the level of artificial diffusivity added to stabilize the simulation. However, in the practical application, alternative strategies may also apply in finding  $\xi$  such as "Doubly Asymptotic Approximation" and "Critical Approximation" [2, 3].*

The 1D strong convection problem  $0.1u_x = u_{xx}$  is simulated by the upwind collocation method. The comparison of the results with the different collocation point locations is provided in Figure 5, where the 1D recursive FEM gradients are employed to verify the collocation distance formulation in Eq. (49). Several cases are presented in this study by varying the position of the collocation points.  $\xi = 0$ , where the collocation points are identical to the nodes, yields a severe oscillatory result; next, when shifting the collocation point to the middle of the upwind nodal representative domain (it is equivalent to shifting 1/4 of the nodal space in this case), as represented by  $\xi = 0.5$ , exhibits a mild diffusive result; furthermore, the collocation points are moved to the boundary of node representative domain (it is the same as the middle of two neighboring nodes), i.e.  $\xi = 1$ , where the points are located at, exhibits no wiggles while the result is not accurate. Finally,  $\xi = 0.61$  based on Eq. (49) serves the optimal collocation point location, which yields a nodally exact solution. The detailed error comparison is further given in Table 1 which confirms that the nodally exact result is achieved by (49).

It is worth noticing that the nodally exact result by the upwind collocation approach only applies to the 1D problem by using the special recursive FEM gradient in Eqs. (46) and (47). For the general case, as one may use different shape functions like IGA and reproducing kernel (RK) approximations, the relationship of collocation point reflected by Eq. (42) may exist in an implicit form. However, using Eq. (49) can still provide a reasonable reference for choosing the collocation points for arbitrary shape functions with acceptable error, which will be later shown in numerical examples from Section 5.

Table 1: Absolute error  $u(x_I) - d_I$  for the 1D collocation with recursive FEM gradients

Point location	$x = 8$	$x = 8.5$	$x = 9$	$x = 9.5$
$\xi = 0$	3.373E-2	7.871E-2	1.836E-1	4.353E-1
$\xi = 0.5$	7.671E-6	1.461E-4	2.724E-3	5.936E-2
$\xi = 1$	9.613E-5	9.705E-4	9.759E-3	9.228E-2
$\xi = 0.61$	1.849E-19	2.213E-19	3.815E-18	2.688E-16

## 4 Upwind reproducing kernel collocation method

Since the existence of the second-order diffusion term in the governing equation, using traditional FEM-type approximation requires special treatment for the second-order derivatives. Although the smoothed FEM gradients introduced in Section 3 can be viewed as an approach to simulate the model problem under a collocation setting, it is non-trivial in generating the concept of second-order FEM gradient into the multi-dimensional situation. The higher order compatibility and smoothness of the meshfree shape function are favorable in developing the upwind collocation scheme in a more general way.

### 4.1 Reproducing Kernel (RK) Approximation

This work employs the reproducing kernel (RK) [8,14] as a model approximation for the simulation under the upwind collocation framework. In RK approximation, the problem domain  $\Omega$  with boundary  $\Gamma$  is discretized by a set of  $NP$

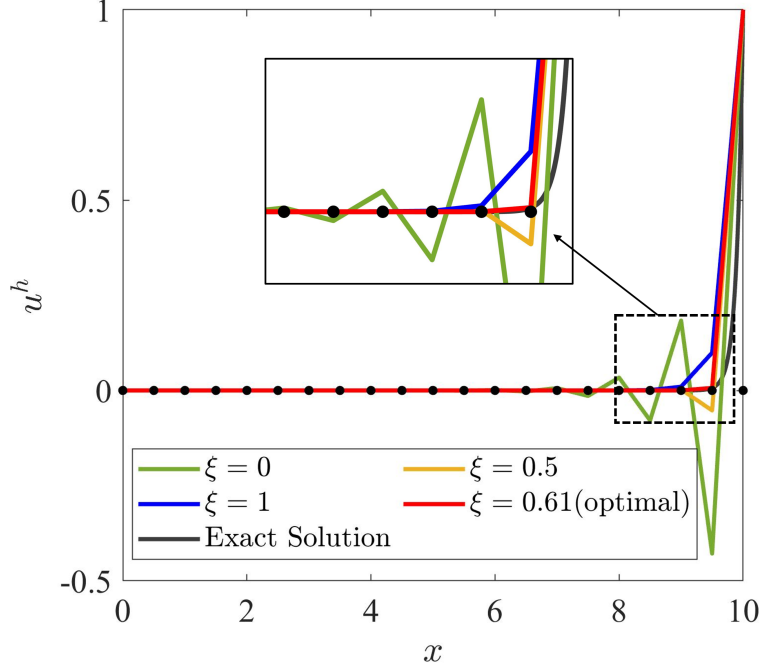


Figure 5: Comparison of different upwind collocation locations by using 1D recursive FEM gradients.

particles. According to the reproducing kernel methodology, the approximation of field variable  $u(\mathbf{x})$ , denoted by  $u^h(\mathbf{x})$ , is expressed as follows:

$$u(\mathbf{x}) \approx u^h(\mathbf{x}) = \sum_{I \in \mathcal{S}_x} \Psi_I(\mathbf{x}) u_I, \quad (52)$$

where  $\Psi_I(\mathbf{x})$  is the RK shape function associated with the  $I$ th meshfree particle under the associated compact support inducing a set of neighbors  $\mathcal{S}_x = \{I | \Psi_I(\mathbf{x}) \neq 0\}$  local to  $\mathbf{x}$ . The RK approximation is first assumed to take the following formulation:

$$\Psi_I(\mathbf{x}) = \mathbf{H}^\top(\mathbf{x} - \mathbf{x}_I) \mathbf{b}(\mathbf{x}) \phi_a(\mathbf{x} - \mathbf{x}_I), \quad (53)$$

where  $\mathbf{H}(\mathbf{x}) = [1, x, y, x^2, \dots, y^p]^\top$  is a column vector of complete  $p$ th order monomials,  $\mathbf{b}(\mathbf{x})$  is a column vector containing all the associated unknown variable coefficients of each component in  $\mathbf{H}$ , and  $\phi_a(\mathbf{x} - \mathbf{x}_I)$  is the kernel function with measure  $a$ , which defines both the locality and order of smoothness in the approximation. The cubic B-spline function is employed in this work to enable a  $C^2$  continuous field:

$$\phi_a(r) = \frac{1}{6} \begin{cases} (2-2r)^3 - 4(1-2r)^3, & r \leq \frac{1}{2} \\ (2-2r)^3, & \frac{1}{2} < r \leq 1 \\ 0, & r > 1 \end{cases}, \quad (54)$$

where  $r \equiv \|\mathbf{x} - \mathbf{x}_I\|/a$  is the normalized relative distance. To obtain the unknown coefficient vector  $\mathbf{b}(\mathbf{x})$ , the following so-called reproducing conditions of the RK shape function  $\Psi(\mathbf{x})$  is enforced to the shape function:

$$\sum_{I \in \mathcal{S}_x} \Psi_I(\mathbf{x}) \mathbf{H}(\mathbf{x}_I) = \mathbf{H}(\mathbf{x}), \quad (55)$$

which is equivalent to the following form with shifted basis:

$$\sum_{I \in \mathcal{S}_x} \Psi_I(\mathbf{x}) \mathbf{H}(\mathbf{x} - \mathbf{x}_I) = \mathbf{H}(\mathbf{0}). \quad (56)$$

Then, the unknown coefficient vector  $\mathbf{b}(\mathbf{x})$  is arrived at by substituting Eq. (53) into Eq. (56), which yields:

$$\mathbf{b}(\mathbf{x}) = \mathbf{M}^{-1}(\mathbf{x}) \mathbf{H}(\mathbf{0}), \quad (57)$$

where  $\mathbf{M}(\mathbf{x}_I) = \sum_{I \in \mathcal{S}_x} \mathbf{H}(\mathbf{x} - \mathbf{x}_I) \mathbf{H}^\top(\mathbf{x} - \mathbf{x}_I) \phi_a(\mathbf{x} - \mathbf{x}_I)$  is the so-called moment matrix. After determining the unknown vector in Eq. (57), substitute it back into the assumed form of the RK shape function (53), one obtains:

$$\Psi_I(\mathbf{x}) = \mathbf{H}^\top(\mathbf{0}) \mathbf{M}^{-1}(\mathbf{x}) \mathbf{H}(\mathbf{x} - \mathbf{x}_I) \phi_a(\mathbf{x} - \mathbf{x}_I). \quad (58)$$



Note that the order of smoothness of  $\Psi_I(\mathbf{x})$  is inherited related by the kernel function  $\phi_a(\mathbf{x} - \mathbf{x}_I)$ . Since the cubic spline kernel function employed is  $C^2$ , the shape function is also  $C^2$ , which is favorable for formulations that require higher-order regularity or smoothness such as strong form collocation.

Substitute the reproducing kernel approximation in (52) to the upwind collocation formulation (32), and the following matrix form is obtained for the upwind reproducing kernel collocation method

$$\tilde{\mathbf{K}}^C \mathbf{u} = \tilde{\mathbf{f}}^C, \quad (59)$$

where the entries of the upwind stiffness matrices and force vector are given by

$$\tilde{K}_{IJ}^C = \begin{cases} \mathbf{a}(\mathbf{x}_C) \cdot \nabla \Psi_J(\mathbf{x}_C) - k \Delta \Psi_J(\mathbf{x}_C), & \mathbf{x}_C \in \mathcal{C}_I \subseteq \tilde{\Omega}_I \\ \mathbf{n} \cdot k \nabla \Psi_J(\mathbf{x}_I), & \mathbf{x}_I \in \Gamma_h \\ \Psi_J(\mathbf{x}_I), & \mathbf{x}_I \in \Gamma_g \end{cases}, \quad (60)$$

$$\tilde{f}_I^C = \begin{cases} s(\mathbf{x}_C), & \mathbf{x}_C \in \mathcal{C}_I \subseteq \tilde{\Omega}_I \\ \bar{h}(\mathbf{x}_I), & \mathbf{x}_I \in \Gamma_h \\ \bar{u}_g(\mathbf{x}_I), & \mathbf{x}_I \in \Gamma_g \end{cases}. \quad (61)$$

## 4.2 Error analysis of upwind reproducing kernel collocation method

The error analysis of the upwind reproducing kernel collocation method is fulfilled by the local truncation error of the discrete system.

**Definition 1.** The local truncation error  $e_I$  associated an interior node  $\mathbf{x}_I$  from Eq. (59) is defined as follows:

$$e_I = \mathbf{a} \cdot \nabla u^h(\mathbf{x}_C) - k \Delta u^h(\mathbf{x}_C) - s(\mathbf{x}_C) = \tilde{K}_{IJ}^C u_J - \tilde{f}_I^C \approx \mathcal{O}(h^p). \quad (62)$$

where  $\mathbf{x}_C \in \mathcal{C}_I \subseteq \tilde{\Omega}_I$  denotes the collocation points for the  $I$ -th row of the system of equations.

**Lemma 1.** The  $\alpha$ -th order derivative of a  $p$ -th order complete reproducing kernel shape function satisfies:

$$\sum_{J \in \mathcal{S}_x} D^\alpha \Psi_J(\mathbf{x}) \mathbf{x}_J^n = D^\alpha \mathbf{x}^n = \frac{n!}{\alpha!} \mathbf{x}^{n-\alpha}, \quad \sum_{J \in \mathcal{S}_x} D^\alpha \Psi_J(\mathbf{x}) (\mathbf{x}_J - \mathbf{x})^n = \begin{cases} \mathbf{0} & n \leq p, \alpha \neq n \\ \alpha! & n \leq p, \alpha = n \end{cases}, \quad (63)$$

where Eq. (63) comes from the direct differentiation of the reproducing conditions of shape function in Eqs. (55) and (56) and  $\alpha$  is the multi-index notation.

**Theorem 1.** For a regular solution  $u \in C^m(\Omega)$ , the local truncation error associated with an interior node for the convection-diffusion problems with the upwind reproducing kernel collocation method with a  $p$ -th order complete shape function is:

$$e_I \approx \mathcal{O}(h^q), \quad q = \min\{p-1, m\}. \quad (64)$$

*Proof.* The local truncation error can be expressed as:

$$\begin{aligned} e_I &= \mathbf{a} \cdot \nabla u^h(\mathbf{x}_C) - k \Delta u^h(\mathbf{x}_C) - s(\mathbf{x}_C) \\ &= [\mathbf{a} \cdot \nabla u^h(\mathbf{x}_C) - k \Delta u^h(\mathbf{x}_C) - s(\mathbf{x}_C)] - \underbrace{[\mathbf{a} \cdot \nabla u(\mathbf{x}_C) - k \Delta u(\mathbf{x}_C) - s(\mathbf{x}_C)]}_{=0} \\ &= \mathbf{a} \cdot [\nabla u^h(\mathbf{x}_C) - \nabla u(\mathbf{x}_C)] - k [\Delta u^h(\mathbf{x}_C) - \Delta u(\mathbf{x}_C)] \\ &= \mathbf{a} \cdot \left[ \sum_{J \in \mathcal{S}_x} \nabla \Psi_J(\mathbf{x}_C) u_J - \nabla u(\mathbf{x}_C) \right] - k \left[ \sum_{J \in \mathcal{S}_x} \Delta \Psi_J(\mathbf{x}_C) u_J - \Delta u(\mathbf{x}_C) \right]. \end{aligned} \quad (65)$$

Taylor's series expansion of  $u_J$  referring to  $u_C$  gives:

$$u_J = \sum_{0 \leq |\alpha| \leq m} \frac{1}{\alpha!} D^\alpha u_C (\mathbf{x}_J - \mathbf{x}_C)^\alpha. \quad (66)$$

The truncation error is then linked with the reproducing condition (56) by bringing Eq. (66) into Eq. (65):

$$\begin{aligned} e_I &= \mathbf{a} \cdot \left[ \sum_{0 \leq |\alpha| \leq m} \frac{1}{\alpha!} D^\alpha u_C \sum_{J \in \mathcal{S}_x} \nabla \Psi_J(\mathbf{x}_C) (\mathbf{x}_J - \mathbf{x}_C)^\alpha - \nabla u(\mathbf{x}_C) \right] \\ &\quad - k \left[ \sum_{0 \leq |\alpha| \leq m} \frac{1}{\alpha!} D^\alpha u_C \sum_{J \in \mathcal{S}_x} \Delta \Psi_J(\mathbf{x}_C) (\mathbf{x}_J - \mathbf{x}_C)^\alpha - \Delta u(\mathbf{x}_C) \right], \end{aligned} \quad (67)$$

with the aid of **Lemma 1**, Eq. (67) reduces to the follows:

$$\begin{aligned}
e_I &= \mathbf{a} \cdot \left[ \sum_{p+1 \leq |\alpha| \leq m} \frac{1}{\alpha!} D^\alpha u_C \sum_{J \in \mathcal{S}_{\mathbf{x}}} \nabla \Psi_J(\mathbf{x}_C) (\mathbf{x}_J - \mathbf{x}_C)^\alpha \right] - k \left[ \sum_{p+1 \leq |\alpha| \leq m} \frac{1}{\alpha!} D^\alpha u_C \sum_{J \in \mathcal{S}_{\mathbf{x}}} \Delta \Psi_J(\mathbf{x}_C) (\mathbf{x}_J - \mathbf{x}_C)^\alpha \right] \\
&= \sum_{p+1 \leq |\alpha| \leq m} \frac{1}{\alpha!} D^\alpha u_C \left[ \mathbf{a} \cdot \sum_{J \in \mathcal{S}_{\mathbf{x}}} \underbrace{\nabla \Psi_J(\mathbf{x}_C)}_{\sim h^{-1}} \underbrace{(\mathbf{x}_J - \mathbf{x}_C)^\alpha}_{\sim h^\alpha} - k \sum_{J \in \mathcal{S}_{\mathbf{x}}} \underbrace{\Delta \Psi_J(\mathbf{x}_C)}_{\sim h^{-2}} \underbrace{(\mathbf{x}_J - \mathbf{x}_C)^\alpha}_{\sim h^\alpha} \right] \\
&\approx \mathcal{O}(h^q), \quad q = \min\{p-1, m\}.
\end{aligned} \tag{68}$$

□

For the problem with smooth solution, Eq. (68) states that the local truncation error for the  $I$ th collocation equation is  $\mathcal{O}(h^{p-1})$ , where  $p$  is the order of reproducing condition of shape function. At least  $(p-1)$ th order convergence rate is guaranteed in the upwind reproducing kernel collocation method regardless of the choice of  $\mathbf{x}_C$ . Furthermore, for the convection-diffusion problems, the special convergence rate can be achieved if the collocation points are the same as the nodal location, i.e.  $\mathbf{x}_C = \mathbf{x}_I$ .

**Lemma 2.** *Under uniform meshfree discretization, the periodicity of reproducing kernel shape function yields the following condition regardless of the order of completeness [27]:*

$$\sum_{J \in \mathcal{S}_{\mathbf{x}}} D^\alpha \Psi_J(\mathbf{x}_C) (\mathbf{x}_J - \mathbf{x}_C)^\alpha = 0, \quad \text{if } (n + \alpha) \text{ is odd, and } \mathbf{x}_C = \mathbf{x}_I. \tag{69}$$

**Theorem 2.** *For a regular solution  $u \in C^m(\Omega)$ , when the collocation points become the nodes, a one-order higher convergence rate is achieved for the convection-diffusion problems when the order of completeness of the shape function  $p$  is an even number:*

$$e_I \approx \mathcal{O}(h^q), \quad q = \min\{p, m\}, \mathbf{x}_C = \mathbf{x}_I \text{ and } p \text{ is even.} \tag{70}$$

*Proof.* With **Lemma 2** and substitute Eq. (69) back to Eq. (68), one has:

$$\begin{aligned}
e_I &= \mathbf{a} \cdot \left[ \sum_{p+1 \leq |\alpha| \leq m} \frac{1}{\alpha!} D^\alpha u_I \sum_{J \in \mathcal{S}_{\mathbf{x}}} \underbrace{\nabla \Psi_J(\mathbf{x}_I)}_{\sim h^{-1}} \underbrace{(\mathbf{x}_J - \mathbf{x}_I)^\alpha}_{\sim h^\alpha} \right] - k \left[ \sum_{p+2 \leq |\alpha| \leq m} \frac{1}{\alpha!} D^\alpha u_I \sum_{J \in \mathcal{S}_{\mathbf{x}}} \underbrace{\Delta \Psi_J(\mathbf{x}_I)}_{\sim h^{-2}} \underbrace{(\mathbf{x}_J - \mathbf{x}_I)^\alpha}_{\sim h^\alpha} \right] \\
&\approx \|\mathbf{a}\| \sum_{p+1 \leq |\alpha| \leq m} \mathcal{O}(h^{\alpha-1}) + k \sum_{p+2 \leq |\alpha| \leq m} \mathcal{O}(h^{\alpha-2}) \\
&\approx \mathcal{O}(h^q), \quad q = \min\{p, m\}.
\end{aligned} \tag{71}$$

□

Finally, for the problem with a smooth solution, by combining Eqs. (68) and (71) the local truncation error of the upwind reproducing kernel collocation method can be summarized as follows:

$$e_I = \begin{cases} \mathcal{O}(h^p), & \mathbf{x}_C = \mathbf{x}_I \text{ and } p \text{ is even} \\ \mathcal{O}(h^{p-1}), & \text{else} \end{cases}. \tag{72}$$

**Theorem 3.** *For a regular solution  $u \in C^m(\Omega)$ , the local truncation error associated with an interior node for the pure convection problems with the upwind reproducing kernel collocation method with a  $p$ -th order complete shape function is:*

$$e_I = \begin{cases} \mathcal{O}(h^{p+1}), & \mathbf{x}_C = \mathbf{x}_I \text{ and } p \text{ is odd} \\ \mathcal{O}(h^p), & \text{else} \end{cases}. \tag{73}$$

The proof for **Theorem 3** is straightforward and followed by setting  $k = 0$  in Eqs. (68) and (71). It can be noticed from Eq. (72) that the convergence rate is reduced when shirting the collocation points from the nodes to the nearby location. To obtain better accuracy, the collocation points are suggested to be the same as the meshfree points if no special stabilization is required for the convection term. According to Eq. (13), the upwind stabilization is necessary when the element Péclet number  $Pe^h > 1$ . Therefore, in practice, the following function is recommended

for turning the upwind stabilization (shifting collocation point from the center to the upwind region) to maintain the entire algorithm as a high-order convergent method when the convection effect is insignificant:

$$\xi = \begin{cases} -1 + 1/Pe^h, & Pe^h < -1 \\ 0, & -1 \leq Pe^h \leq 1 \\ 1 - 1/Pe^h, & Pe^h > 1 \end{cases} . \quad (74)$$

### 4.3 Alternative treatment of second order diffusion term by finite volume approximation

Since the existence of the diffusion term, the second-order reproducing condition is necessary to have a convergent result. However, the requirement of higher order completeness causes additional effort for building shape functions.

In the collocation framework, significant efforts have been devoted to the development of the collocation approach by only employing the linear shape functions. In [27], Wang et. al. classified the convergence of the collocation method with linear shape function as a special property called "Superconvergent" in the collocation method. It has been identified that the extra higher-order reproducing condition is possessed by the low-order shape function under whatever special treatments enable this superconvergent behavior.

Similarly, the treatment of second-order diffusion term can also be treated by a finite volume type technique with the use of only linear shape function. Thus, the reproducing kernel finite volume method is obtained by approximating the second-order derivative of the shape function in Eq. (60) by:

$$\Delta\Psi(\mathbf{x}_C) \approx \tilde{\Delta}\Psi(\mathbf{x}_C) = \frac{1}{V_I} \int_{\Omega_I} \Delta\Psi(\mathbf{x})d\Omega = \frac{1}{V_I} \int_{\Gamma_I} \nabla\Psi(\mathbf{x}) \cdot \mathbf{n}d\Gamma, \quad (75)$$

where the divergence theorem has been employed to Eq. (75). Thus, the entire collocation equation does not need the calculation of the second-order derivatives of the shape function.

**Theorem 4.** *Eq. (75) satisfies extra quadratic reproducing conditions under uniform node distribution when only the linear basis function is employed for computing the shape function under uniform node distribution:*

$$\sum_{J \in \mathcal{S}_x} \Delta\tilde{\Psi}_J(\mathbf{x}) \tilde{\mathbf{H}}(\mathbf{x}_J) = \Delta\tilde{\mathbf{H}}(\mathbf{x}), \quad (76)$$

where

$$\tilde{\mathbf{H}}(\mathbf{x}) = \{x^2, xy, y^2\}^T. \quad (77)$$

Now for the smooth problem, the RKFM formulation can achieve  $e_I = \mathcal{O}(h)$  when only the linear basis is employed. The proof of **Theorem 4** will be provided in the Appendix.

## 5 Numerical Examples

In this section, several 1D and 2D numerical examples will be presented to validate the effectiveness of the proposed upwind collocation scheme. The related formulations that will be employed in numerical comparisons are provided in Table 2. The reproducing kernel collocation method is abbreviated as RKCM, in which the collocation points are meshfree nodes themselves. The inconsistent RKCM refers to the formulation with only the first-order gradients of the field variable treated by the upwind way. The rest of the terms are all collocated at the original nodal position. The consistent upwind reproducing kernel collocation method is termed "Upwind RKCM", which is the proposed formulation to provide stabilized simulation results. Last, the upwind reproducing kernel finite-volume method (Upwind RKFM) represents an alternative approach where the diffusion term is approximated by the finite-volume type approximation. The choice of support size in the reproducing kernel approximation has been studied over the years. In general, the order of convergence in the Galerkin type meshfree method and the point collocation meshfree method does not depend on the choice support size [27, 32, 33]. The minimum requirement of support size in RK approximation is given in [32]. Sometimes, a slightly larger support may deliver better accuracy. Nevertheless, excessively large support sizes may lead to a much more diffusive result. In the present work, our major concentration is the selection of the evaluation points. When a nonuniform layout of collocation points is determined, a relatively larger support size may be applied to meet the minimum requirement in [32].

Table 2: List of abbreviations

Abbreviation	Formulation
RKCM	$\mathbf{a}(\mathbf{x}_I) \cdot \nabla u^h(\mathbf{x}_I) = k\Delta u^h(\mathbf{x}_I) + s(\mathbf{x}_I)$
Inconsistent upwind RKCM	$\mathbf{a}(\mathbf{x}_I) \cdot \nabla u^h(\mathbf{x}_C) = k\Delta u^h(\mathbf{x}_I) + s(\mathbf{x}_I)$
Upwind RKCM	$\mathbf{a}(\mathbf{x}_C) \cdot \nabla u^h(\mathbf{x}_C) = k\Delta u^h(\mathbf{x}_C) + s(\mathbf{x}_C)$
Upwind RKFM	$\mathbf{a}(\mathbf{x}_C) \cdot \nabla u^h(\mathbf{x}_C) = k\tilde{\Delta}u^h(\mathbf{x}_C) + s(\mathbf{x}_C)$

### 5.1 1D pure convection problem with piecewise linear source

The first numerical example is the pure convection problem taken from [34] with the infinite element Péclet number  $Pe^h = \infty$  as the consequence of zero diffusivity. This test aims to verify the consistency of the proposed upwind RKCM. It will address a long-standing concern regarding upwind techniques, which tend to demonstrate reduced accuracy when handling source terms. The strong form of the problem is:

$$\begin{cases} vu_{,x} = s, & x \in ]0, L] \\ u(0) = 0 \end{cases}, \quad (78)$$

where  $L = 15$ , and  $v = 1$  are employed in this example. The body force  $s$  is given as a piecewise linear function:

$$s = \begin{cases} 1 - \frac{15}{4L}x, & x \leq \frac{2}{5}L \\ \frac{15}{4L}(x - \frac{8L}{15}), & \frac{2}{5}L < x \leq \frac{8}{15}L \\ 0, & \frac{8}{15}L < x \leq L \end{cases}. \quad (79)$$

The three different collocation schemes that will be used in the simulation are illustrated in Figure 6(a), where the case  $\xi = 0$  brings the upwind RKCM back to the traditional RKCM. Since the absence of diffusion term, the suggested collocation point for this problem is  $\xi = 1$ , which indicates that the collocation points should be located on the boundary of the nodal representative domain. The inconsistent upwind RKCM is added to represent the collocation scheme with only the treatment to the first-order gradients of the field variable, and another upwind RKCM case with  $\xi = 0.5$  is provided as the consistent upwind RKCM without the proper selection of collocation points. The linear basis function with normalized support size 1.6 is employed in the reproducing kernel approximation. From Figure 6(b), the inconsistent upwind yields the worst result, which produces the same phenomenon as results in [34]. The RKCM, which is analogous to the central difference scheme, yields good agreement of the exact solution as it is supposed to be, and no oscillation has been observed as a consequence of lacking the diffusion term. The upwind RKCM with  $\xi = 0.5$  represents yields a relatively large error, which confirms the fact that the collocation point in this case is not the optimal choice. Finally, when  $\xi = 1$ , the simulation yields the best result, which verifies the consistency of the proposed methodology and the concept of choosing the collocation point based on the element Péclet number. A convergence comparison for this 1D pure convection problem with source term is illustrated in Figure 7, where 16, 31, 46, 61, and 76 uniformly distributed particles are employed in this study. As expected, due to the inconsistency formulation, the upwind RKCM without collocating the source term on the evaluation points yielded the worst accuracy. Meanwhile, the upwind RKCM with  $\xi = 0.5$  gives a convergent solution but lost accuracy. Since the absence of diffusivity, the RKCM without shifting collocation points to the upwind side also delivered a good result, which is comparable to the upwind RKCM with  $\xi = 1$ . The  $L_2$  rate of RKCM is one order higher than the others, which is consistent with the error analysis (73).  $H_1$  error norm remains as the first order, which is a result of the interpolation error with linear complete shape function [32, 35]. It is worth noticing that upwind RKCM with  $\xi = 1$  also delivered a one-order higher convergence rate. The reason behind this phenomenon is that the collocation points in this case are set to be the middle of each neighbor node pair, which makes the formulation satisfy (69). However, we claim that this only belongs to a special case of (69), as the constant convection speed and zero diffusivity in this problem have made the evaluation points to be the mid-points.

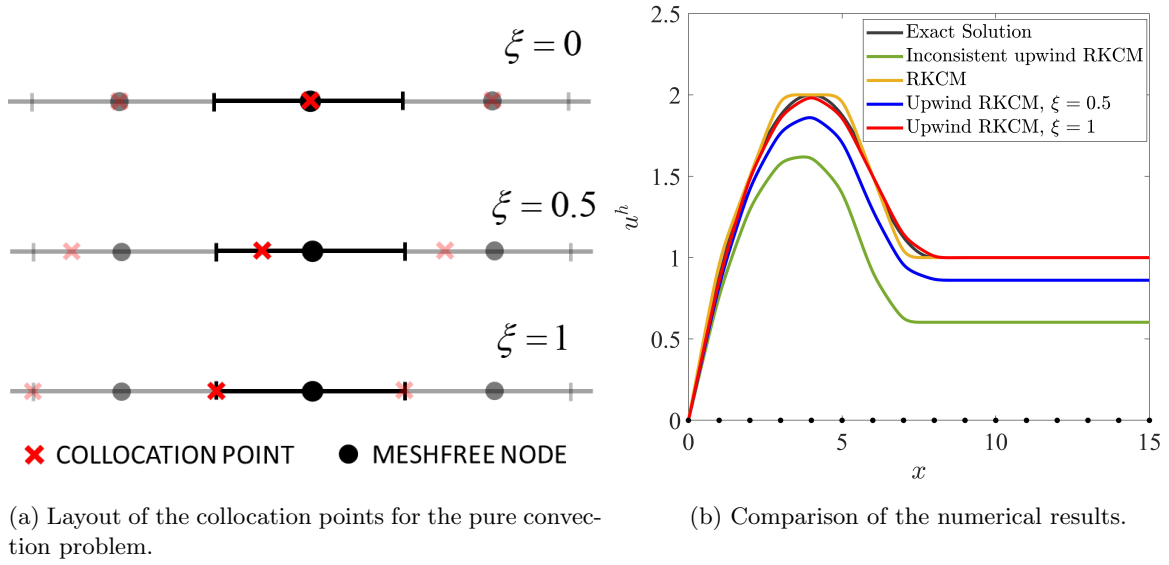


Figure 6: Comparison of numerical results for the 1D pure convection problem by different collocation schemes.

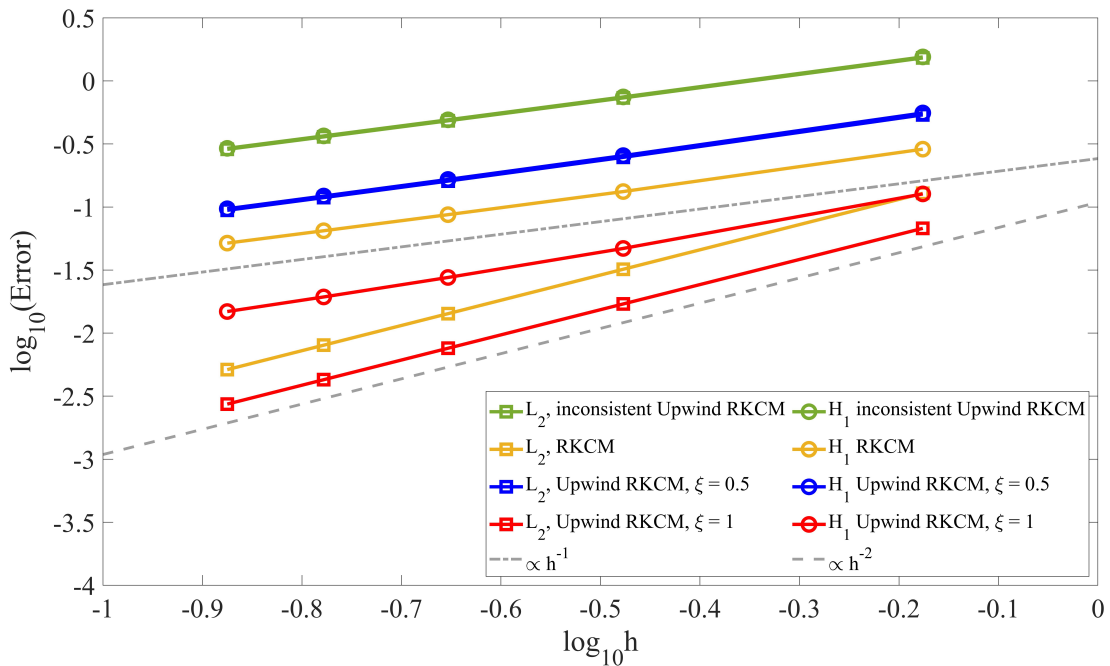


Figure 7: Comparison of the convergence rate for the 1D pure convection problem by different collocation schemes.

## 5.2 1D convection-diffusion problem

Reconsider the 1D convection-diffusion problem with the following governing equation:

$$\begin{cases} vu_{,x} = ku_{,xx}, & x \in ]0, L[ \\ u(0) = 0 \\ u(L) = 1 \end{cases}, \quad (80)$$

where  $L = 10$ ,  $k = 0.05$ , and  $v = 1$ . The element Péclet number is  $Pe^h = 5$  based on the 21 uniformly distributed meshfree particles. The linear basis with normalized support size 1.5 is employed in building the RK shape function in Galerkin-based RKPM and collocation-based RKFM. For RKCM, since the minimum requirement of approximation basis is quadratic, we employ the quadratic basis with normalized support size 2.3 in this case. The selection of the location of the collocation is based on (74). As shown in Figure 8, both RKPM, RKCM, and RKFM exhibit oscillatory results as the stability requirement is not satisfied. By shifting the collocation points from the nodal points to the desired upwind points, the solutions become stable and are closer to the exact solution for both upwind RKCM and RKFM.

A convergence study for the different choices of the upwind collocation points is provided in Figure 9, where 11, 21, 41, 81, and 161 uniformly distributed meshfree particles are employed for the calculation of the error norms. We term Eq. (49) as "Hyperbolic tangent" and Eq. (74) as "Critical approximation". Both approaches deliver at least a linear convergence rate in  $L_2$  and  $H_1$ , which is consistent with the error analysis in Section 4.2. As observed from Figure 9(a), these two approaches yield identical results when the discretization is coarse. As the model is refined, "critical approximation" gives the better accuracy. This is because when the element Péclet number is smaller than 1, Eq. (74) will lead the collocation points to be the same as the nodal location. From Eq. (70), one has better accuracy when  $\mathbf{x}_c = \mathbf{x}_I$ . The relative collocation distance is depicted in Figure 9(b), which confirms the error analysis provided in Section 4.2.

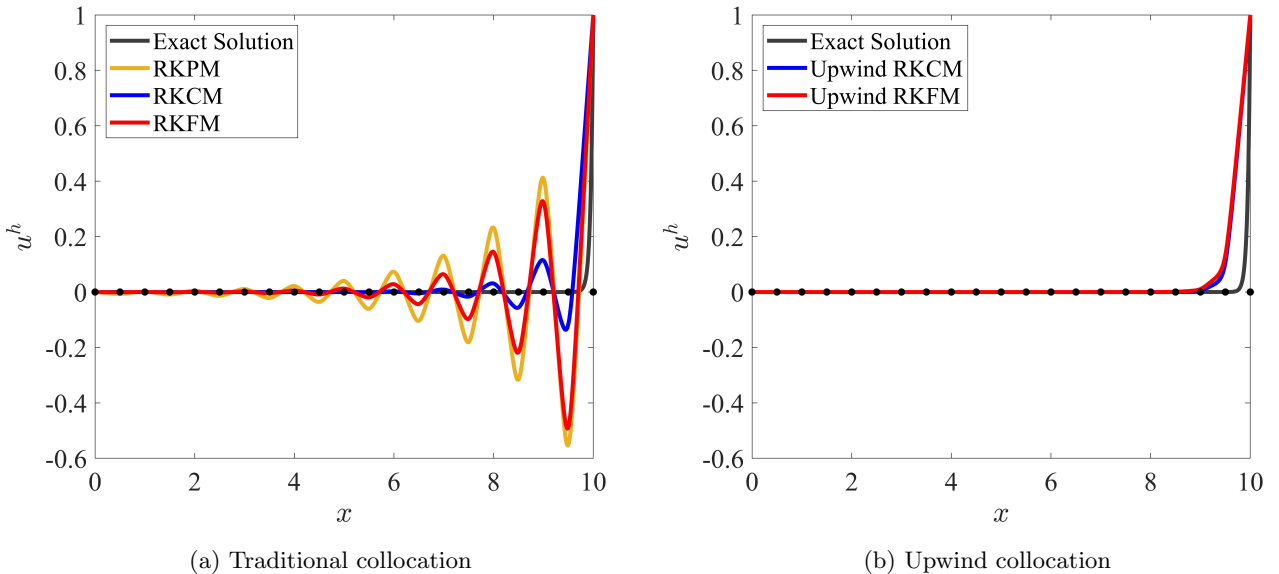
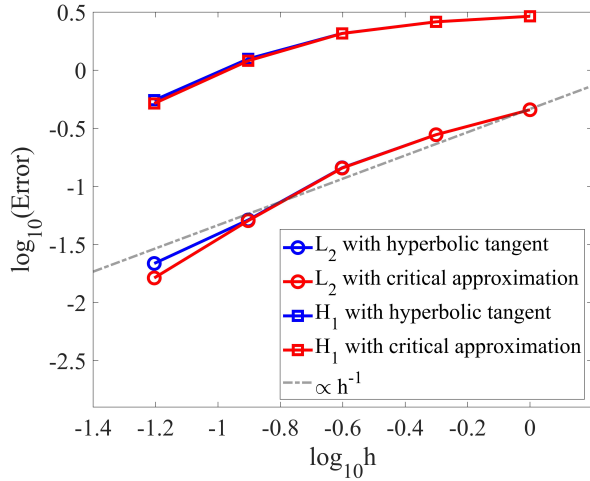


Figure 8: Comparison of unstabilized numerical schemes (left) with the upwind stabilized schemes (right) for the 1D convection-diffusion problem with 21 uniformly distributed particles,  $\xi = 0.8$ .

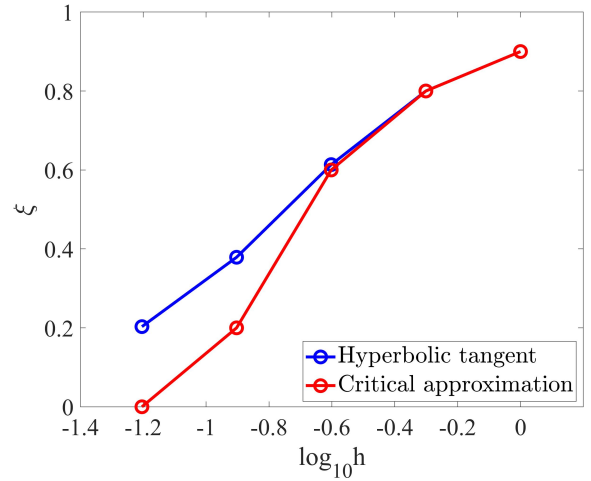
## 5.3 2D strong convection problem: flow skew to mesh

Next, the 2D example is presented to examine the crosswind wiggles in the proposed upwind collocation method. The 2D problem is defined in  $[0, 1] \times [0, 1]$  with zero source term. The diffusivity is set as  $k = 10^{-6}$  to present a strong convection setup [31]. The velocity is given by  $\mathbf{a} = \{\cos \theta, \sin \theta\}$ , where  $\theta$  is the flow direction. The quadratic basis function with normalized support size 2.3 is adopted in RKCM, and the linear basis function with support size 1.5 is used for RKFM in this example. Uniformly distributed  $41 \times 41$  particles is utilized to test three cases with flow direction  $\theta = \pi/6$ ,  $\theta = \pi/4$ , and  $\theta = \pi/3$ . The layout for the collocation point is provided in Figure 10.

The first case is shown in Figure 11, where the Dirichlet boundary conditions are enforced on  $x = 0$  and  $y = 0$  and the outflow boundaries are given on  $x = 1$  and  $y = 1$ . The exact solution to this problem is the advection of the inflow boundary condition in the flow direction [3]. The comparison of simulation results under different flow directions is



(a) Error norm of upwind RKCM



(b) Relative collocation distance by different evaluation functions

Figure 9: Comparison of the convergence rate for the 1D convection-diffusion problem with upwind RKCM.

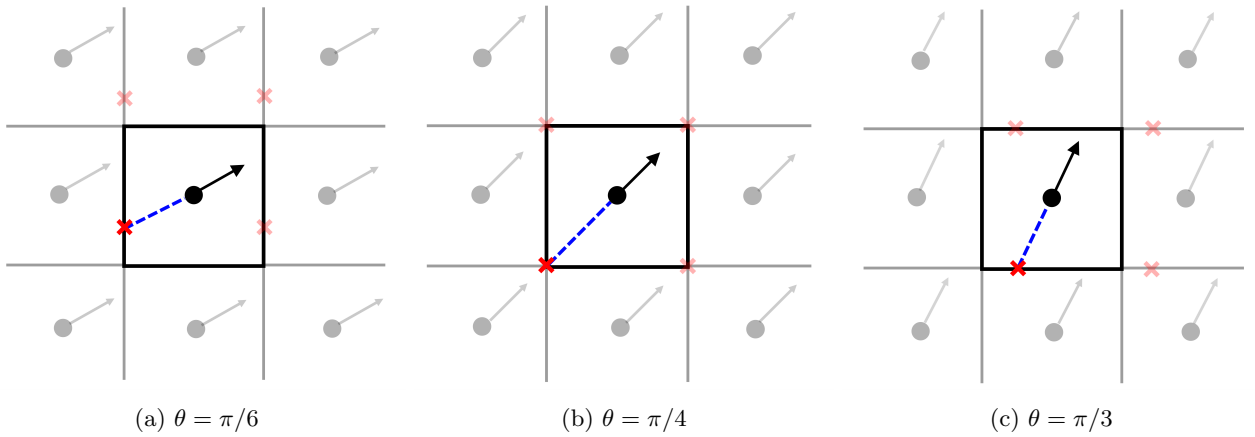


Figure 10: Collocation schemes of 2D strong convection problem for the different flow angles.

given in Figure 12. The traditional RKCM with the collocation points being the RK nodes yields oscillations and large errors. By using the upwind treatment to the convection term, stable results can be found from both upwind RKFM and upwind RKCM.

The second case considers the same problem setup but with all the boundaries being the Dirichlet boundary conditions, which are shown in Figure 13. The existence of the boundary layer makes severe oscillations for the traditional collocation RKCM, which is illustrated in Figure 14. Both upwind RKCM and RKFM yield stable results, and no crosswind effect is observed in the present algorithm. Meanwhile, RKCM exhibits less diffusive results than RKFM.

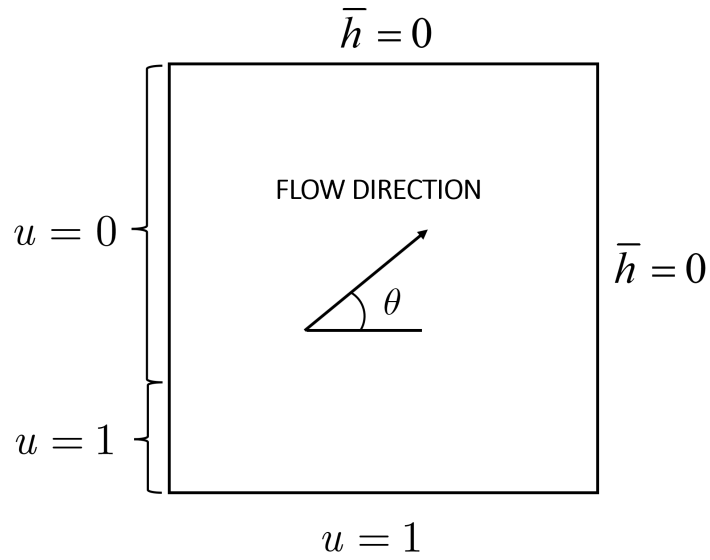


Figure 11: Description of the 2D strong convection problem with convection skew to mesh: outflow boundary at  $x = 1$  and  $y = 1$ .

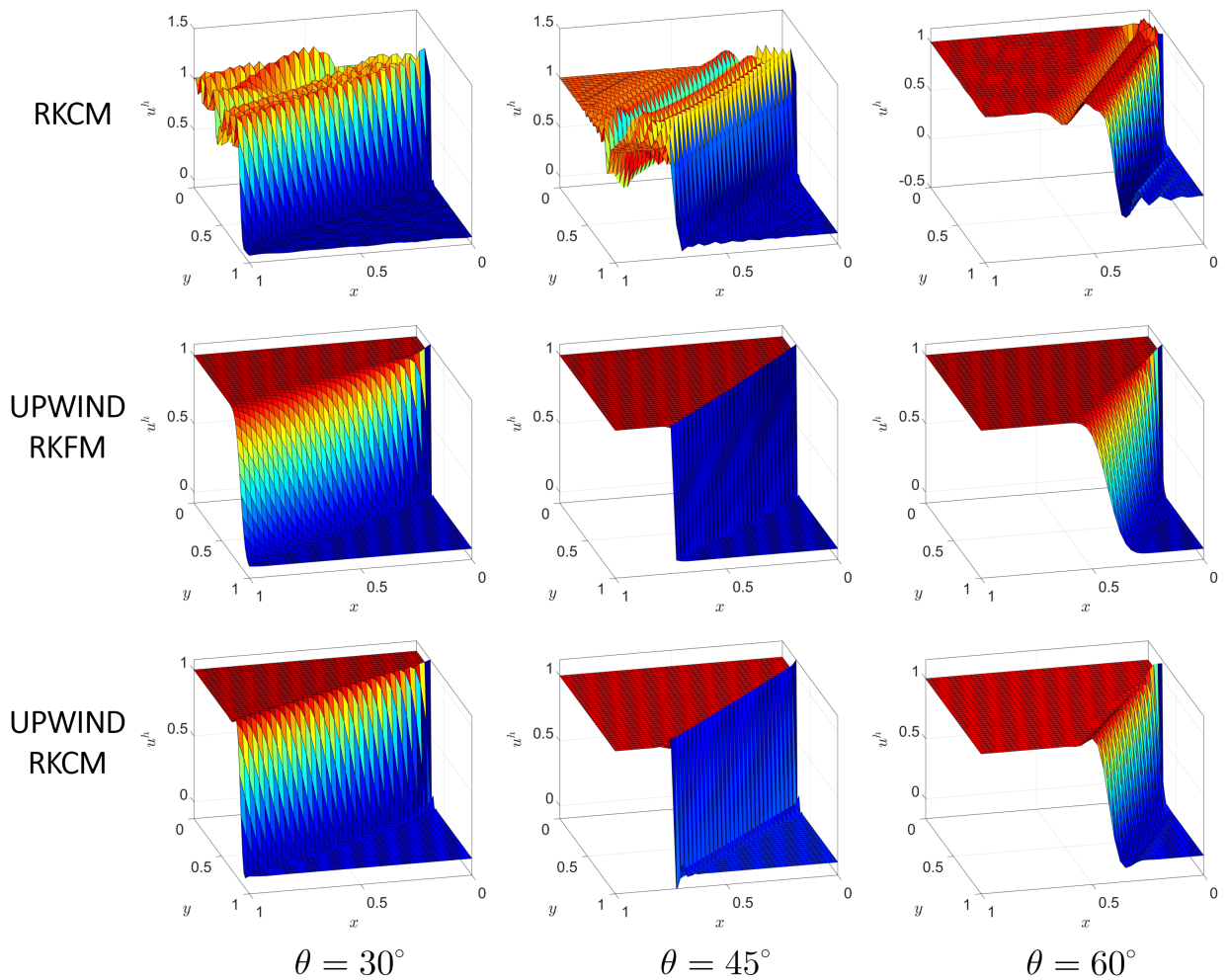


Figure 12: Comparison of 2D strong convection problem: outflow boundary at  $x = 1$  and  $y = 1$ .



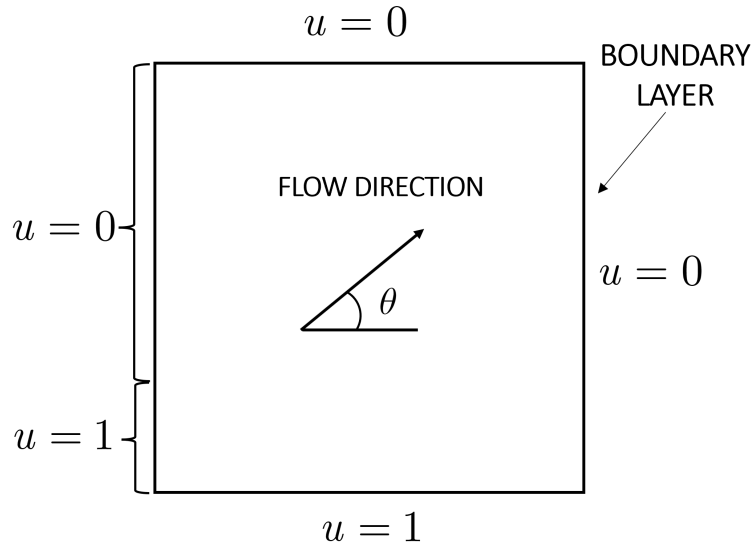


Figure 13: Description of the 2D strong convection problem with convection skew to mesh: Dirichlet boundary at  $x = 1$  and  $y = 1$ .

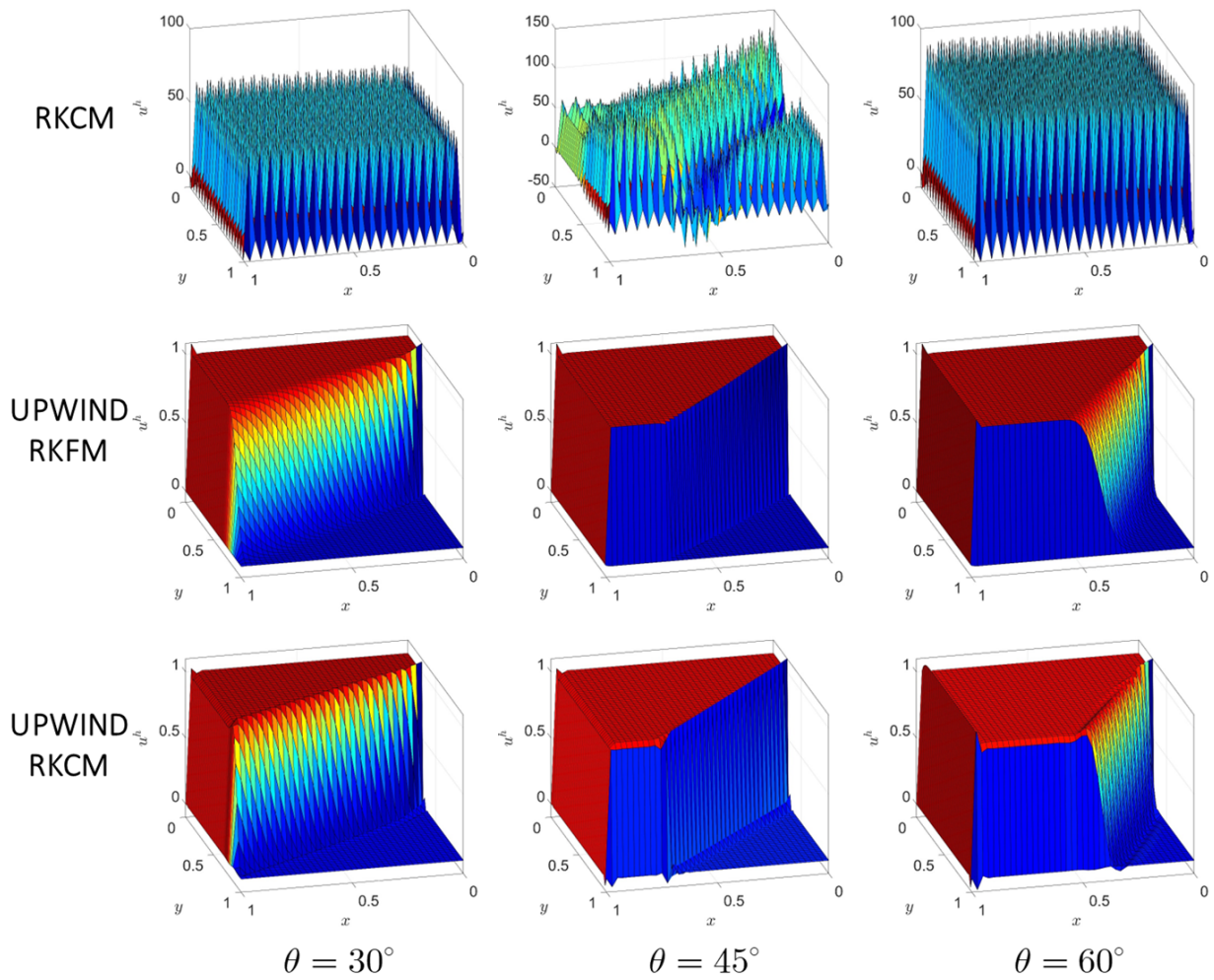


Figure 14: Comparison of 2D strong convection problem: pure Dirichlet boundary conditions.

## 5.4 2D cosine hill in a rotating field

A rotation field with variable velocity  $\mathbf{a} = \{-y, x\}$  on the bi-unit domain  $[-0.5, 0.5] \times [-0.5, 0.5]$  is considered in Figure 15 with  $s = 0$  and a constant diffusivity  $k = 10^{-6}$  to make problem as convection-dominated. The homogeneous Dirichlet boundary conditions are prescribed on the boundary of the domain. In addition, a prescribed essential boundary condition is enforced along section O-A, as given in Fig. 15(a). The layout of the collocation points for the  $21 \times 21$  uniformly distributed particles is illustrated in Figure 15(b). The cosine hill along O-A is given as:

$$\bar{u}(\mathbf{x}) = 0.5(\cos(4\pi y + \pi) + 1.0). \quad (81)$$

The convection term makes the internal boundary O-A transport along the circular streamline. A quadratic basis function with a normalized support size of 2.5 is used for reproducing kernel approximation.

The comparison of field variables is provided in Figure 16. The RKCM exhibits acceptable results with slight oscillation near the boundary, as shown in Figure 16(a). Another simulation is performed with only the convection term being treated by upwind methodology; the flow velocity is still evaluated at the nodal location, which is termed as inconsistent upwind RKCM. In Figure 16(b), the crosswind diffusion effect can be observed under the inconsistent upwind RKCM. Finally, the upwind RKCM produces very good simulation results, as shown in Figure 16(c).

Next, a convergence test is performed for the cosine hill problem with  $11 \times 11$ ,  $21 \times 21$ ,  $41 \times 41$ , and  $81 \times 81$  particles, where an initial random perturbation of particles (15% nodal space) is applied on  $11 \times 11$  case. Both uniform and nonuniform cases are considered and the nonuniform particle refinement is shown in Figure 17. The related collocation points for the nonuniform case are selected based on characteristic nodal space, which is obtained by calculating the distance of the nearest neighbor point to each node. The analytical solution can be approximately considered as follows:

$$u(\mathbf{x}) = \begin{cases} 0.5(\cos(4\pi r + \pi) + 1.0), & r < 0.5 \\ 0, & \text{else} \end{cases}, \quad (82)$$

where  $r = (x^2 + y^2)^{0.5}$  is the radius from the origin. From Figure 18(a), RKCM and upwind RKCM both yield convergent results for the uniform refinement, which are consistent with the error analysis. Since the quadratic complete RK shape functions are employed in both cases,  $L_2$  error norms are second order as a result of small diffusivity. The upwind RKCM produces better accuracy than the traditional RKCM, which is consistent with the observation from Figure 16. The first-order convergent results are also observed from the nonuniform convergence test, which is shown in Figure 18(b). The upwind RKCM demonstrated better accuracy compared to the traditional RKCM.

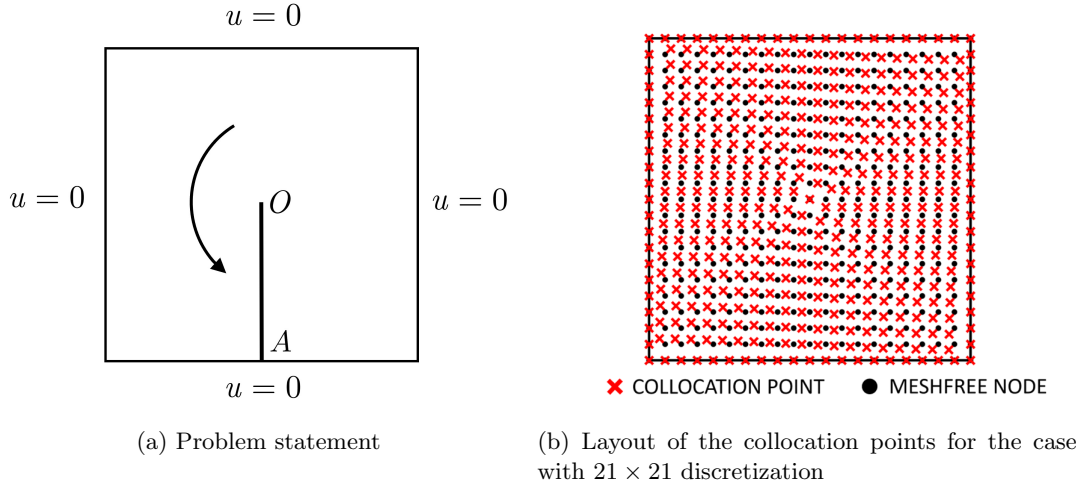


Figure 15: Problem statement of the 2D cosine hill in a rotating flow field.

## 5.5 Cone impinging on a natural boundary

The previously derived upwind reproducing kernel collocation method can be easily extended to the transient case. The collocation formulation for an interior point is then stated as:

$$\dot{u}(\mathbf{x}_C, t) + \mathbf{a}(\mathbf{x}_C, t) \cdot \nabla u(\mathbf{x}_C, t) = k\Delta u(\mathbf{x}_C, t) + s(\mathbf{x}_C, t). \quad (83)$$

The unconditionally stable generalized trapezoidal rule [1, 3] (GTR) is employed for the time integration:

$$u_{n+1} = u_n + \frac{\Delta t}{2}(\dot{u}_n + \dot{u}_{n+1}). \quad (84)$$

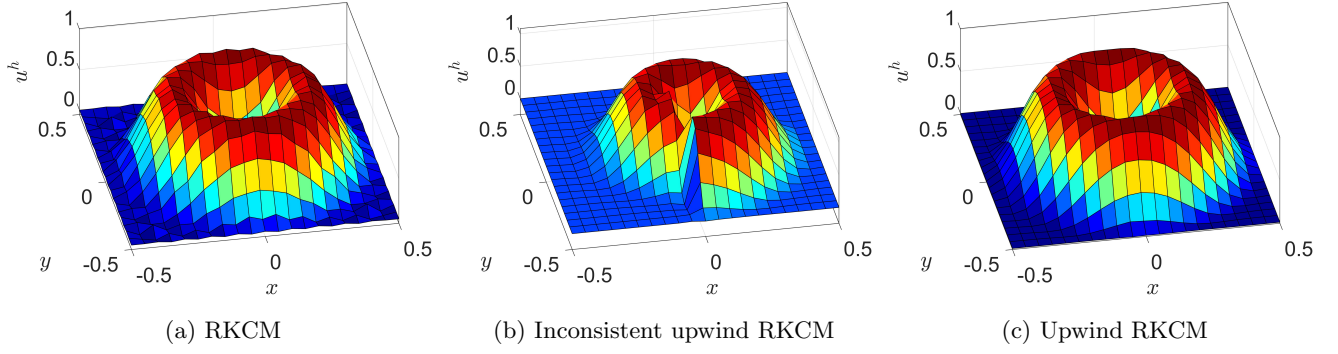


Figure 16: Comparison of rotating flow field for the 2D cosine hill problem for the case with  $21 \times 21$  discretization.

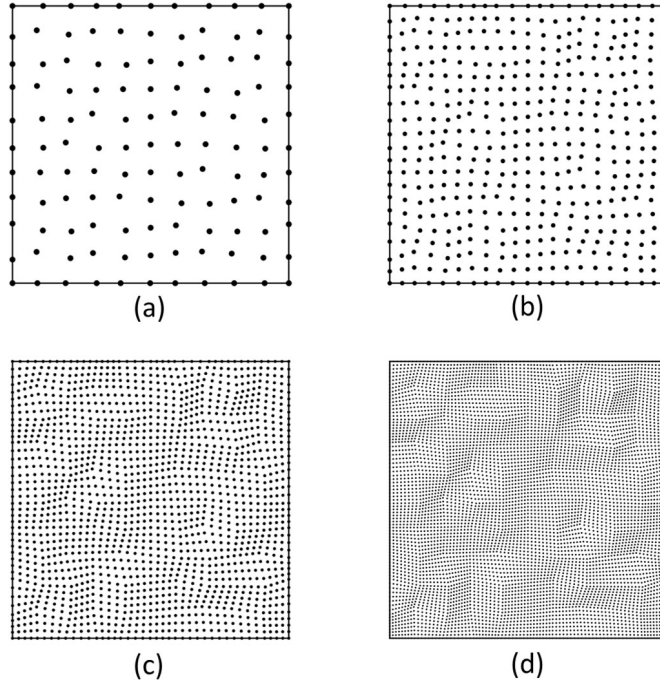


Figure 17: Nonuniform discretizations for the convergence test of the 2D cosine hill problem: (a)  $11 \times 11$  particles; (b)  $21 \times 21$  particles; (c)  $41 \times 41$  particles; (d)  $81 \times 81$  particles.

where  $u_{n+1} = u(\mathbf{x}, t_{n+1})$  and  $\Delta t$  is the time step. The transient problem is therefore solved by the implicit setting. The problem is setup in Figure 19 and modeled in  $[-1.5, 1.5] \times [-0.5, 0.5]$  with  $61 \times 21$  reproducing kernel particles. The diffusivity and source term are set as 0 to make the problem diffusion-free. The convection velocity is  $\mathbf{a} = \{1, 0\}$ . The time step is chosen as  $\Delta t = 0.01$ , which finally makes the Courant number to the fully discretized problem as  $\text{Cr} = 0.2$ . The cosine cone provided in section 5.3 is employed as the initial condition centered at  $(-1, 0)$ . The reproducing kernel approximation adopts the linear basis function with normalized support size 2.0.

The comparison between the traditional RKCM and upwind RKCM is detailed in Figure 20. The oscillation appears at the upwind side of traditional RKCM and exists after the cone hits the natural boundary (3.5% of the height of the cone). The relatively small oscillation can be observed from the upwind RKCM at the downwind side when the cone is translating over the interior domain. No oscillation remains in the problem domain after impinging on the natural boundary ( $10^{-8}\%$  of the height of the cone remains in the problem domain).

Next, the convergence study is provided in Figure 21. First, the effect of temporal discretization is investigated. Since the time integration is unconditionally stable, we decrease the time step of the problem with discretization provided in Figure 19(b). Although no blowing-up simulation results are observed, the dissipation error is evidently shown in the case with a larger time step  $\Delta t = 0.05$ . The Courant number associated with this case is  $\text{Cr} = 1$ . With a decreased time step, the wiggles are shifted from the upwind side to the downwind side. The downwind wiggles can occasionally be observed in the linear upwind scheme with high-order accuracy and can be reduced by refining the discretization. Next, we employed a small time step to the problem and studied the refinement in space for this problem, where  $h_x$  denotes the nodal space over  $x$ -direction. Three uniformly distributed particle sets with the

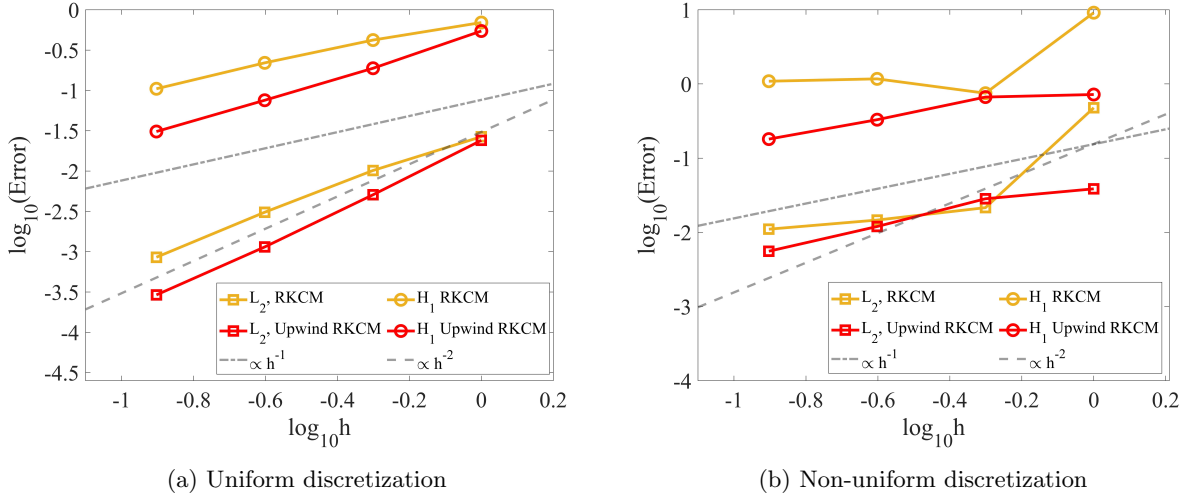


Figure 18: Comparison of the convergence rate for the 2D cosine hill problem.

discretization  $61 \times 21$ ,  $121 \times 41$ , and  $181 \times 61$  are utilized. As observed in Figure 21, a series of decreased spatial discretizations can successfully reduce the downwind wiggles and again, no upwind wiggles are presented, which is further confirmed by the comparison of the height of the cone in Table 3, where the reference height value is 1.

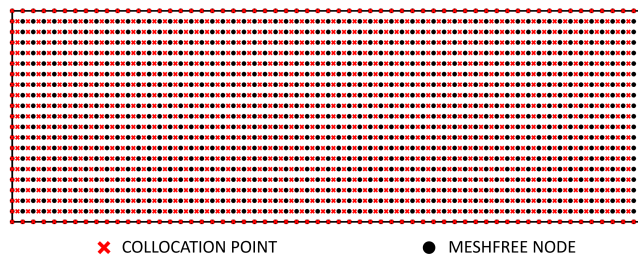
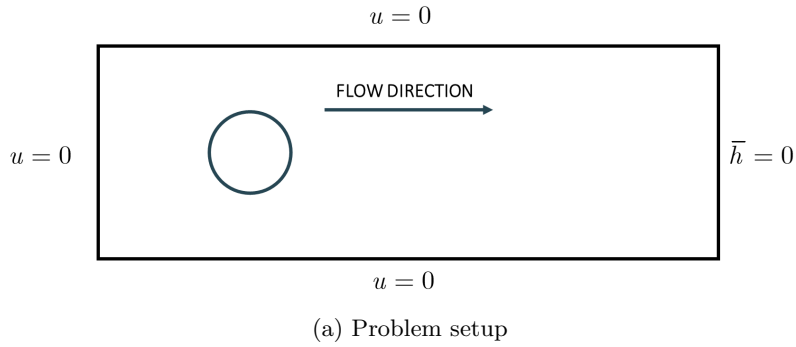


Figure 19: Problem description of the cone impinges a natural boundary.

## 5.6 2D rotating field

Finally, the 2D transient problem with a rotating field is provided. The problem setup is shown in Figure 22 in domain  $[-0.5, 0.5] \times [-0.5, 0.5]$ . The discretization and collocation points are chosen as in 5.4. The velocity is given by  $\mathbf{a} = (-y, x)$  with zero diffusivity. The initial condition is identical to the cosine cone used in the example section 5.5. The linear basis function with normalized support size 2.0 is employed in RK approximation. No source term is considered and the time step is selected as  $\Delta t = 0.01$ .

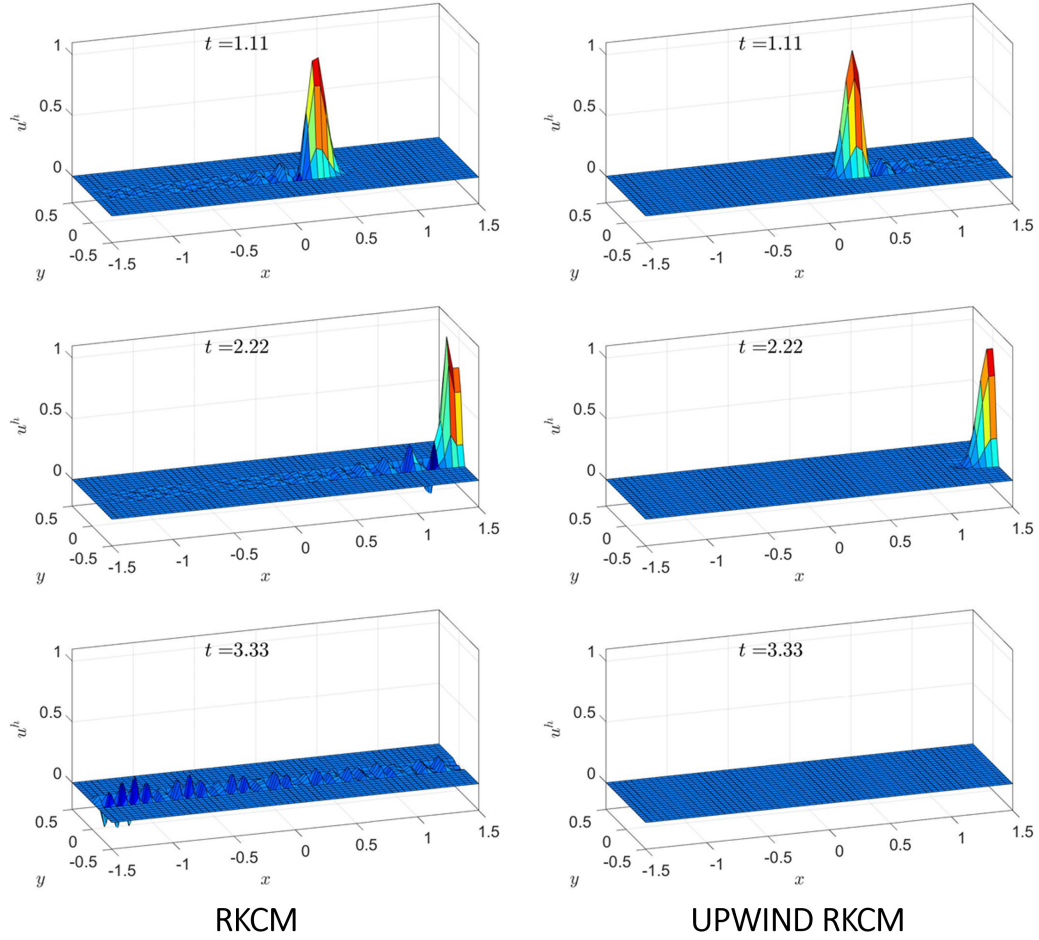


Figure 20: Comparison of cone impinging a natural boundary at various time.

Table 3: Comparison of the height of the cone impinging a natural boundary problem at time  $t = 1.11$  using upwind RKCM (reference value 1)

Upwind RKCM	$h_x = 0.05$	$h_x = 0.025$	$h_x = 0.017$
$\Delta t = 0.05$	0.7480	0.7975	0.8145
$\Delta t = 0.01$	0.8641	0.9508	0.9833
$\Delta t = 0.002$	0.8568	0.9802	0.9854



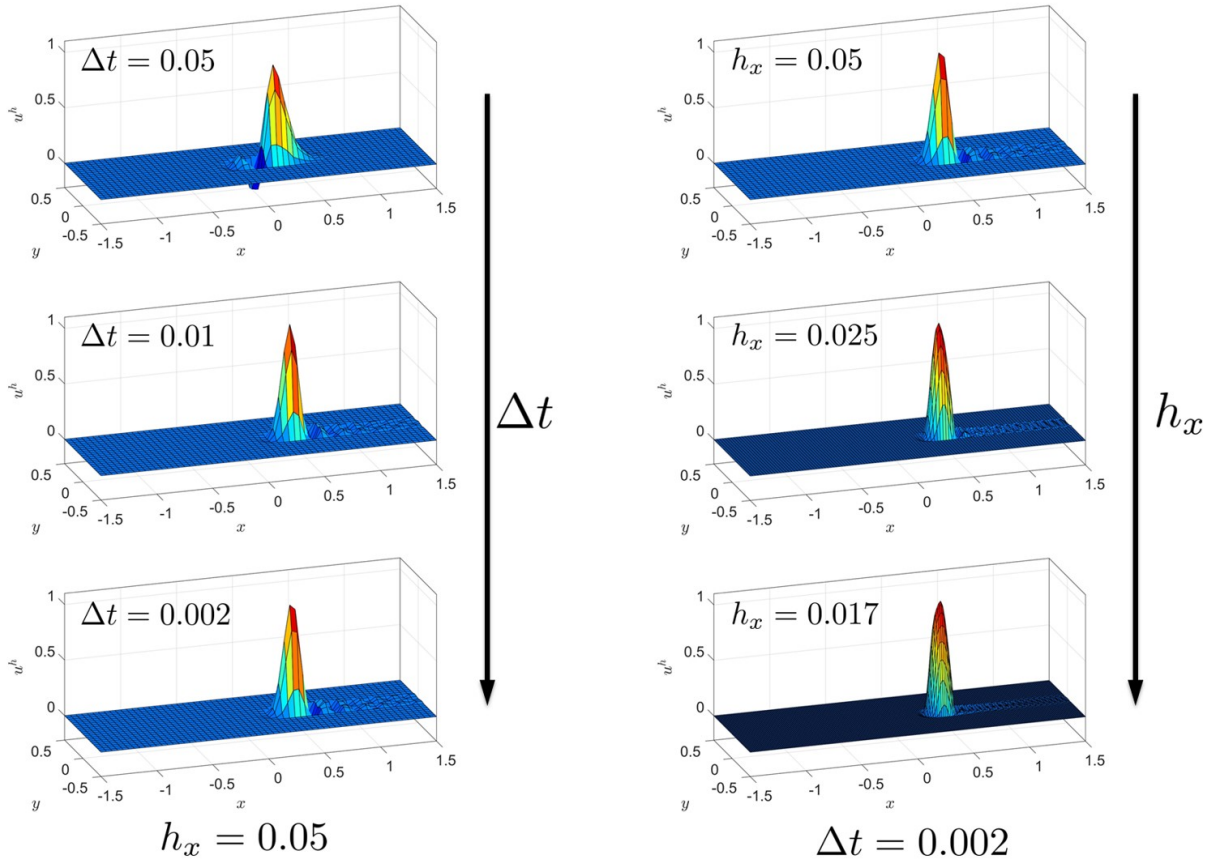


Figure 21: Comparison of cone impinging a natural boundary at time  $t = 1.11$  under spatial and temporal refinements.

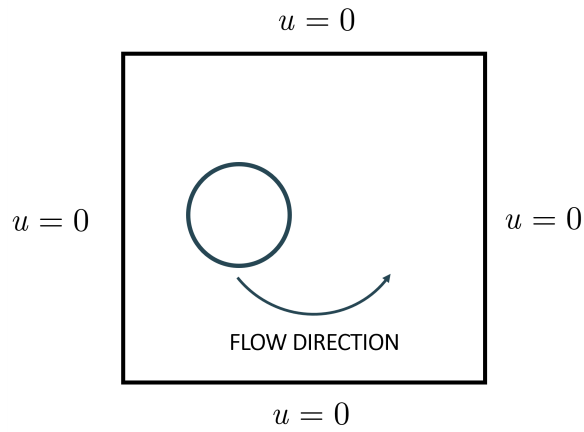


Figure 22: Problem statement of a cosine cone in a rotating field.

The results comparison of RKCM and upwind RKCM is shown in Figure 23. The traditional RKCM yields virtually no dissipation, but the phase error is present after two full rotations. The upwind oscillations are observed and exist in the problem domain during the rotation. On the contrary, upwind RKCM delivers good results. No upwind wiggles exist in the problem domain, and a slight downwind effect is presented. The comparison of the height of the cone for the upwind RKCM is given in Table 4, where the reference height is 1. As observed in the table, the dissipation is observed when the discretization of the problem is coarse. As the model is refined, upwind RKCM delivers little dissipation error.

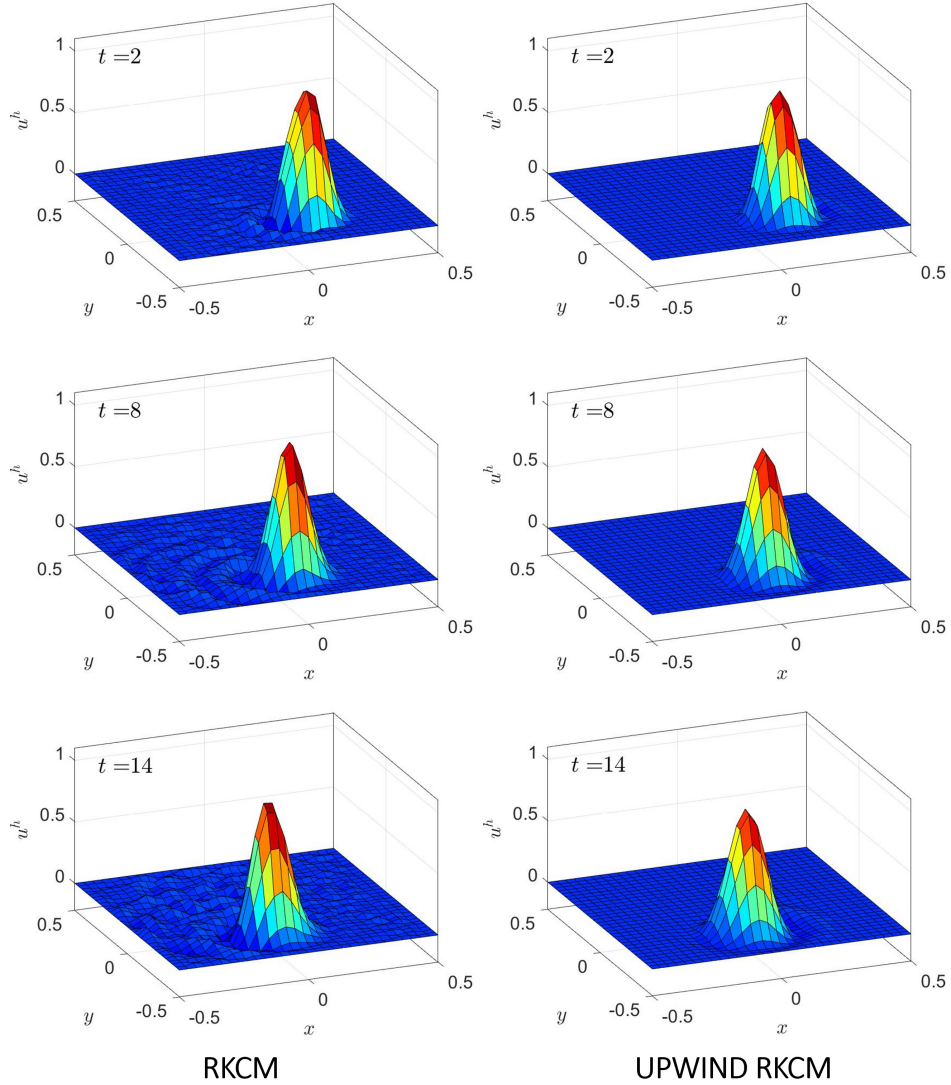


Figure 23: Comparison of 2D rotating cone problem after two full rotations.

Table 4: Comparison of the height of the rotating cone problem under various discretizations using upwind RKCM (reference value 1)

Upwind RKCM	$t = 2$	$t = 8$	$t = 14$
$h_x = 0.01$	0.8610	0.7598	0.6953
$h_x = 0.05$	0.9529	0.9885	0.9936
$h_x = 0.025$	0.9895	0.9936	0.9939

## 6 Conclusions and discussions

A general upwind reproducing kernel collocation method is proposed for convection-dominated problems. The non-self-adjoint nature of these problems necessitates Petrov-Galerkin approaches. However, it's worth noting that, when

using the traditional meshfree collocation method, severe oscillations can still occur if upwind stabilization is not applied.

We began with a 1D finite difference scheme and established a connection between finite differences and the concept of gradient smoothing in the meshfree method literature. Our systematic analysis has demonstrated that traditional finite difference stencils can be reinterpreted as contour integrals of finite element shape functions over a representative domain. This innovative perspective brings the connection between the finite difference and the continuous approximation in these numerical methods.

Subsequently, we developed a specialized upwind stabilization technique for convection-dominated problems by employing gradient smoothing over the convection term. Our analysis revealed that selecting the smoothing domain as the upwind region of each nodal representative domain is crucial for achieving upwind stabilization. We then designed the upwind reproducing kernel collocation method, utilizing evaluation points at the upwind side of each nodal representative domain. The precise location of these collocation points is determined by the element Péclet number, eliminating the need for artificial parameters in the entire upwind collocation framework. An error analysis demonstrated that the upwind reproducing kernel collocation method possesses  $O(h^{p-1})$ th order convergence rate, where  $p$  is the degree of basis function in approximation. Finally, our proposed upwind reproducing kernel collocation method demonstrated strong performance in both steady and unsteady convection-dominated examples.

We've identified that our proposed method's stabilization structure is linear (independent of the numerical solution), setting it apart from nonlinear schemes like SUPG. The choice of order of completeness in the shape function can be arbitrary. This linear scheme offers flexibility in choosing the order of completeness for shape functions, making it adaptable for high-order accuracy. The choice of support size in reproducing kernel approximation extends the connection between particles and their neighbors. Larger support sizes can occasionally lead to slight downwind oscillations in coarse discretizations, which can be mitigated by increasing the number of discretization points. Moreover, our method shows potential for application in modeling the Navier-Stokes equation and fluid-structure-interaction (FSI) problems. The convection term in the N-S equation is time-dependent and may require additional effort to shift the evaluation points in time, which will be considered as part of our future plans.

**Acknowledgements** This work was supported by the National Science Foundation award number 1826221 to the Pennsylvania State University. J. Wang would like to thank Prof. Chi-Wang Shu at from

## Appendix

In this Appendix, we would like to show that the second-order gradients produced by the RKFM formulation satisfy the relevant consistency condition and thus can achieve  $e_I = \mathcal{O}(h)$  when only the linear basis is employed. First, Eq. (75) can be rewrite as follows:

$$\tilde{\Delta}\Psi_J(\mathbf{x}) = \frac{1}{V_I} \int_{\Gamma_I} \mathbf{n} \cdot \nabla \Psi_J(\mathbf{x}) \, d\Gamma := \sum_K \chi_K(\mathbf{x}) \cdot \nabla \Psi_J(\mathbf{x}_K) = \sum_K \left( \frac{A_K}{V_I} \mathbf{n}(\mathbf{x}_K) \right) \cdot \nabla \Psi_J(\mathbf{x}_K), \quad \mathbf{x} \in \Omega_I, \quad (85)$$

where the numerical quadrature has been carried out to (85), the quadrature points are denoted by  $\mathbf{x}_K$ , and  $A_K$  represents the area of the  $K$ th surface or weight of  $\mathbf{x}_K$ .

**Lemma 3.** *When the numerical quadrature to (85) is sufficiently accurate, the following special properties can be derived for  $\chi_K(\mathbf{x})$ :*

$$\sum_K \chi_K(\mathbf{x}) = \frac{1}{V_I} \sum_K \mathbf{n}(\mathbf{x}_K) A_K = \frac{1}{V_I} \int_{\Gamma_I} \mathbf{n} \, d\Gamma = \{0, 0\}^T, \quad (86)$$

$$\sum_K \chi_K(\mathbf{x}) x_K = \frac{1}{V_I} \sum_K \mathbf{n}(\mathbf{x}_K) A_K x_K = \frac{1}{V_I} \int_{\Gamma_I} x \mathbf{n} \, d\Gamma = \frac{1}{V_I} \int_{\Omega_I} \{1, 0\}^T \, d\Omega = \{1, 0\}^T. \quad (87)$$

The proof of **Theorem 4** is given as follows:

*Proof.* Consider the second-order consistency condition of  $\tilde{\Psi}_{I,xx}$  with only the employment of linear basis function,



we have:

$$\begin{aligned}
\sum_{J \in \mathcal{S}_{\mathbf{x}}} \tilde{\Psi}_{J,xx}(\mathbf{x}) x_J^2 &= \sum_{J \in \mathcal{S}_{\mathbf{x}}} \sum_K \chi_{K1}(\mathbf{x}) \Psi_{J,x}(x_K) (x_J - x_K + x_K)^2 \\
&= \sum_{J \in \mathcal{S}_{\mathbf{x}}} \sum_K \chi_{K1}(\mathbf{x}) \Psi_{J,x}(x_K) x_K^2 + 2 \sum_{J \in \mathcal{S}_{\mathbf{x}}} \sum_K \chi_{K1}(\mathbf{x}) \Psi_{J,x}(x_K) (x_J - x_K) x_K \\
&\quad + \sum_{J \in \mathcal{S}_{\mathbf{x}}} \sum_K \chi_{K1}(\mathbf{x}) \Psi_{J,x}(x_K) (x_J - x_K)^2 \\
&= \sum_K \chi_{K1}(\mathbf{x}) x_K^2 \underbrace{\sum_{J \in \mathcal{S}_{\mathbf{x}}} \Psi_{J,x}(\mathbf{x}_K)}_{=0} + 2 \sum_K \chi_{K1}(\mathbf{x}) x_K \underbrace{\sum_{J \in \mathcal{S}_{\mathbf{x}}} \Psi_{K,x}(\mathbf{x}_K)}_{=1} (x_J - x_K) \\
&\quad + \sum_J \chi_{J1}(\mathbf{x}) \sum_{I \in \mathcal{S}_{\mathbf{x}}} \Psi_{I,x}(\mathbf{x}_J) (x_I - x_J)^2 \\
&= 2 \underbrace{\sum_K \chi_{K1}(\mathbf{x}) x_K}_{=1 \text{ from (87)}} + \sum_K \chi_{K1}(\mathbf{x}) \sum_{J \in \mathcal{S}_{\mathbf{x}}} \Psi_{J,x}(\mathbf{x}_K) (x_J - x_K)^2 \\
&= 2 + \sum_K \chi_{K1}(\mathbf{x}) \sum_{J \in \mathcal{S}_{\mathbf{x}}} \Psi_{J,x}(\mathbf{x}_K) (x_J - x_K)^2,
\end{aligned} \tag{88}$$

where  $\chi_{K1}(\mathbf{x}) = n_1(\mathbf{x}_K) A_K / V_I$  denotes the first component of  $\chi_K(\mathbf{x})$  and Eq. (87) has been employed. Now, if the shape function  $\Psi$  is building under the quadratic basis function, the last term in Eq. (88) is exactly 0. However, when only a linear basis is employed, if the particle discretization is uniform without the boundary truncation effect, the summation  $\sum_{I \in \mathcal{S}_{\mathbf{x}}} \Psi_{I,x}(\mathbf{x}_J) (x_I - x_J)^2$  remains a constant value over the interior domain. Thus, Eq. (88) becomes to:

$$\sum_{J \in \mathcal{S}_{\mathbf{x}}} \tilde{\Psi}_{J,xx}(\mathbf{x}) x_J^2 = 2 + \sum_{J \in \mathcal{S}_{\mathbf{x}}} \Psi_{J,x}(\mathbf{x}_K) (x_J - x_K)^2 \underbrace{\sum_K \chi_{K1}(\mathbf{x})}_{=0 \text{ from (86)}} = 2. \tag{89}$$

The consistency condition of the second-order finite-volume type gradients with respect to  $xy$  and  $y^2$  can also be obtained by a similar procedure.  $\square$

Since the derivation of Eq. (89) does not require the quadratic basis function, the condition provided via (89) is so-called extra high order consistency [27]. Finally, with the extra high-order reproducing condition, the upwind collocation method with finite-volume type treatment of the second-order diffusion term under only linear basis function can achieve a similar convergence rate as the upwind RKCM with quadratic basis function.

## References

- [1] T. J. Hughes, The Finite Element Method: Linear Static and Dynamic Finite Element Analysis, Courier Corporation, 2012.
- [2] I. Christie, D. F. Griffiths, A. R. Mitchell, O. C. Zienkiewicz, Finite element methods for second order differential equations with significant first derivatives, International Journal for Numerical Methods in Engineering 10 (6) (1976) 1389–1396.
- [3] A. N. Brooks, T. J. Hughes, Streamline upwind/Petrov-Galerkin formulations for convection dominated flows with particular emphasis on the incompressible Navier-Stokes equations, Computer Methods in Applied Mechanics and Engineering 32 (1-3) (1982) 199–259.
- [4] T. J. Hughes, L. P. Franca, G. M. Hulbert, A new finite element formulation for computational fluid dynamics: Viii. the Galerkin/least-squares method for advective-diffusive equations, Computer Methods in Applied Mechanics and Engineering 73 (2) (1989) 173–189.
- [5] T. J. Hughes, G. R. Feijóo, L. Mazzei, J.-B. Quincy, The variational multiscale method—a paradigm for computational mechanics, Computer methods in applied mechanics and engineering 166 (1-2) (1998) 3–24.
- [6] F. Brezzi, A. Russo, Choosing bubbles for advection-diffusion problems, Mathematical Models and Methods in Applied Sciences 4 (04) (1994) 571–587.

- [7] J.-S. Chen, M. Hillman, S.-W. Chi, Meshfree methods: progress made after 20 years, *Journal of Engineering Mechanics* 143 (4) (2017) 04017001.
- [8] J.-S. Chen, C. Pan, C.-T. Wu, W. K. Liu, Reproducing kernel particle methods for large deformation analysis of non-linear structures, *Computer Methods in Applied Mechanics and Engineering* 139 (1-4) (1996) 195–227.
- [9] P. Guan, S. Chi, J. Chen, T. Slawson, M. Roth, Semi-lagrangian reproducing kernel particle method for fragment-impact problems, *International Journal of Impact Engineering* 38 (12) (2011) 1033–1047.
- [10] J.-S. Chen, C.-T. Wu, S. Yoon, Y. You, A stabilized conforming nodal integration for Galerkin mesh-free methods, *International Journal for Numerical Methods in Engineering* 50 (2) (2001) 435–466.
- [11] M. Hillman, J.-S. Chen, An accelerated, convergent, and stable nodal integration in Galerkin meshfree methods for linear and nonlinear mechanics, *International Journal for Numerical Methods in Engineering* 107 (7) (2016) 603–630.
- [12] E. Oñate, S. Idelsohn, O. Zienkiewicz, R. Taylor, C. Sacco, A stabilized finite point method for analysis of fluid mechanics problems, *Computer Methods in Applied Mechanics and Engineering* 139 (1-4) (1996) 315–346.
- [13] W. K. Liu, S. Jun, D. T. Sihling, Y. Chen, W. Hao, Multiresolution reproducing kernel particle method for computational fluid dynamics, *International Journal for Numerical Methods in Fluids* 24 (12) (1997) 1391–1415.
- [14] W. K. Liu, S. Jun, Y. F. Zhang, Reproducing kernel particle methods, *International Journal for Numerical Methods in Fluids* 20 (8-9) (1995) 1081–1106.
- [15] H. Lin, S. Atluri, Meshless local Petrov-Galerkin(MLPG) method for convection diffusion problems, *CMES(Computer Modelling in Engineering & Sciences)* 1 (2) (2000) 45–60.
- [16] T.-P. Fries, H. G. Matthies, A stabilized and coupled meshfree/meshbased method for the incompressible Navier–Stokes equations—part I: stabilization, *Computer Methods in Applied Mechanics and Engineering* 195 (44-47) (2006) 6205–6224.
- [17] Y. Gu, G.-R. Liu, Meshless techniques for convection dominated problems, *Computational Mechanics* 38 (2) (2006) 171–182.
- [18] Y. Chan, L. Shen, C. Wu, D. Young, A novel upwind-based local radial basis function differential quadrature method for convection-dominated flows, *Computers & Fluids* 89 (2014) 157–166.
- [19] D. Yun, Y. Hon, Improved localized radial basis function collocation method for multi-dimensional convection-dominated problems, *Engineering Analysis with Boundary Elements* 67 (2016) 63–80.
- [20] P. L. Roe, Approximate Riemann solvers, parameter vectors, and difference schemes, *Journal of Computational Physics* 43 (2) (1981) 357–372.
- [21] C. Shu, H. Ding, H. Chen, T. Wang, An upwind local rbf-dq method for simulation of inviscid compressible flows, *Computer Methods in Applied Mechanics and Engineering* 194 (18-20) (2005) 2001–2017.
- [22] M. Hillman, J.-S. Chen, Nodally integrated implicit gradient reproducing kernel particle method for convection dominated problems, *Computer Methods in Applied Mechanics and Engineering* 299 (2016) 381–400.
- [23] S.-W. Chi, J.-S. Chen, H.-Y. Hu, J. P. Yang, A gradient reproducing kernel collocation method for boundary value problems, *International Journal for Numerical Methods in Engineering* 93 (13) (2013) 1381–1402.
- [24] T.-H. Huang, Stabilized and variationally consistent integrated meshfree formulation for advection-dominated problems, *Computer Methods in Applied Mechanics and Engineering* 403 (2023) 115698.
- [25] N. Aluru, A point collocation method based on reproducing kernel approximations, *International Journal for Numerical Methods in Engineering* 47 (6) (2000) 1083–1121.
- [26] S. Chi, J. Chen, H. Luo, H. Hu, L. Wang, Dispersion and stability properties of radial basis collocation method for elastodynamics, *Numerical Methods for Partial Differential Equations* 29 (3) (2013) 818–842.
- [27] D. Wang, J. Wang, J. Wu, Superconvergent gradient smoothing meshfree collocation method, *Computer Methods in Applied Mechanics and Engineering* 340 (2018) 728–766.

- [28] D. Wang, J. Wang, J. Wu, Arbitrary order recursive formulation of meshfree gradients with application to superconvergent collocation analysis of Kirchhoff plates, *Computational Mechanics* 65 (3) (2020) 877–903.
- [29] T. J. Hughes, J. A. Cottrell, Y. Bazilevs, Isogeometric analysis: CAD, finite elements, NURBS, exact geometry and mesh refinement, *Computer Methods in Applied Mechanics and Engineering* 194 (39-41) (2005) 4135–4195.
- [30] P. M. Gresho, R. L. Lee, Don't suppress the wiggles—they're telling you something!, *Computers & Fluids* 9 (2) (1981) 223–253.
- [31] T. J. Hughes, A simple scheme for developing 'upwind' finite elements, *International Journal for Numerical Methods in Engineering* 12 (9) (1978) 1359–1365.
- [32] W. Han, X. Meng, Error analysis of the reproducing kernel particle method, *Computer Methods in Applied Mechanics and Engineering* 190 (46-47) (2001) 6157–6181.
- [33] J. Wu, D. Wang, An accuracy analysis of Galerkin meshfree methods accounting for numerical integration, *Computer Methods in Applied Mechanics and Engineering* 375 (2021) 113631.
- [34] B. Leonard, A survey of finite differences of opinion on numerical muddling of the incomprehensible defective confusion equation, *Finite Element Methods for Convection Dominated flows* 34 (1979) 1–17.
- [35] L. Deng, D. Wang, An accuracy analysis framework for meshfree collocation methods with particular emphasis on boundary effects, *Computer Methods in Applied Mechanics and Engineering* 404 (2023) 115782.